CENTRO DE INVESTIGACIÓN Y DE ESTUDIOS AVANZADOS DEL INSTITUTO POLITÉCNICO NACIONAL

UNIDAD ZACATENCO
DEPARTAMENTO DE CONTROL AUTOMÁTICO

"Identificación de los parámetros de un servomecanismo equipado con un amortiguador magnetoreológico considerando la flexibilidad"

T E S I S

Presentado por

JUAN MANUEL MARTÍN DEL CAMPO RODRÍGUEZ

Para obtener el grado de

MAESTRO EN CIENCIAS

En la especialidad de

CONTROL AUTOMÁTICO

Director de Tesis: Rubén Alejandro Garrido Moctezuma

Ciudad de México Febrero 2018

CENTRO DE INVESTIGACIÓN Y DE ESTUDIOS AVANZADOS DEL INSTITUTO POLITÉCNICO NACIONAL

UNIDAD ZACATENCO
DEPARTAMENTO DE CONTROL AUTOMÁTICO

"Parameter identification of a servomechanism equipped with a magnetorheological damper and considering the flexibility"

T H E S I S

Submitted by

JUAN MANUEL MARTÍN DEL CAMPO RODRÍGUEZ

To Obtain the Degree of

MASTER OF SCIENCE

In the Field of

AUTOMATIC CONTROL

Thesis Supervisor: Rubén Alejandro Garrido Moctezuma

Mexico City February 2018

AGRADECIMIENTOS

Agradezco al Consejo Nacional de Ciencia y Tecnología (CONACYT) por el apoyo otorgado a través la beca de posgrado para la realización de este trabajo de tesis.

Agradezco también al Dr. Rubén Alejandro Garrido Moctezuma por la orientación y ayuda brindada como director de este trabajo.

Quiero agradecer a los sinodales, el Dr. Moisés Bonilla Estrada y Dr. Ieroham Solomon Barouh por el tiempo dedicado a la revisión de este proyecto y por sus comentarios.

Finalmente, quiero agradecer también a los ingenieros Gerardo Castro y Jesús Meza por su ayuda en la configuración del prototipo de laboratorio utilizado.

ACKNOWLEDGEMENT

I thank Consejo Nacional de Ciencia y Tecnología (CONACyT) for its support through the posgraduate scholarship to accomplish this thesis work.

I am grateful to PhD Rubén Alejandro Garrido Moctezuma, for its guidance and help provided as thesis supervisor.

I appreciate the advisers, PhD Moisés Bonilla Estrada and PhD Ieroham Solomon Barouh for the time devoted to review this work and for their comments

Finally, I also thank engineers Gerardo Castro and Jesús Meza for their help in settting up the laboratory testbed.

RESUMEN

El objetivo de este trabajo es desarrollar metodologías de indentificación de parámetros aplicadas a un servomecanismo acoplado a un amoritguador magnetoreológico (MD), tomando en cuenta las flexibilidades. Se consideran 3 casos. El primer caso corresponde al servomecanismo acoplado a una carga y a un MD que no se encuentra excitado. El segundo caso es una variante del primero, con el MD excitado con diferentes voltajes. En el tercer caso, una segunda inercia es acoplada al servomecanismo por medio de un resorte introduciendo así flexiblidad, además el MD se mantiene sin excitación. Se emplean dos metodologías para la identificación de parámetros. La primera es el Método de Identificación con Filtros de Estado (SFIM), que utiliza un algoritmo de Mínimos Cuadrados fuera de línea y genera un vector regresor por medio de filtros lineales de estado. Por su parte, la segunda metodología de identificación es el Método de Identificación Recursivo Algebraico (ARIM) y emplea un vector regresor producido por medio de técnicas de cálculo operacional acopladas a un algoritmo de Mínimo Cuadrados Recursivo. En el primer caso, el SFIM es aplicado a un model que considera sólo la fricción viscosa mientras que el ARIM se aplica a un modelo de cuatro parámetros. El segundo y tercer caso consideran sólo el modelo de cuatro parámetros. Los experimentos en tiempo real del segundo caso muestran que el modelo de cuatro parámetros coinciden con los datos experimentales sólo para valores bajos de excitación aplicados al MD. Por otra parte, las simulaciones respaldan los resultados de la identificación paramétrica en el tercer caso.

ABSTRACT

The goal of this work is to develop parameter identification methodologies applied to a servomechanism coupled to a magnetorheological damper (MD) and considering flexibilities. Three cases are considered. The first case corresponds to the servomechanism coupled to an inertial load and to a MD. Here, the MD is not excited. The second case is a variant of the first case when the MD is excited through different voltages. In the third case, a second inertial load is coupled to the servomechanism by means of a spring, thus introducing flexibilities and the MD is not excited. Two methodologies are employed for parameter identification. The first methodology called the State Filter Identification Method, resorts on an off-line Least Squares algorithm, and the corresponding regressor vector is generated by linear state filters. The second parameter identification methodology, the Algebraic Recursive Identification Method (ARIM), employs a regressor vector, produced by means of Operational Calculus techniques, coupled to a Recursive Least Squares algorithm. In the first case, the SFIM is applied to a model considering only viscous friction, and the ARIM is applied to a four-parameter model. The second and third cases consider only the four-parameter model. The real-time experiments in the second case shows that the four-parameter model fits adequately the experimental data only for low excitation voltages applied to the MD. On the other hand, numerical experiments support the parameter identification in the third case.

CONTENTS

List of figures **III**

List of tables **V**

1 Introduction **1**

2 Experimental setup **7**

3 Parameter identification of the prototype without considering flexibility **11**

3.1 Prototype Section 1 model 11

3.2 Parameter identification 15

3.2.1 Filter State Identification Method (FSIM) 15

3.2.2 Algebraic Recursive Identification Method (ARIM) 18

3.3 Experimental comparison between the FSIM and the ARIM algortihms . 22

3.3.1 Model validation 23

3.3.2 Experimental results 26

3.4 Change of the parameters estimates due to magnetorheological damping 30

4 Parameter identification of the prototype considering flexibility **33**

4.1 Prototype Section 1 plus Section 2 model 33

4.2 Parameter identification 36

4.3 Stabilization of the system 40

4.4 Simulation setting 44

4.5 Results 45

4.5.1 Remarks 48

5 Conclusions **51**

Appendices **53**

A Magnetorheological damper 55

B System parameterization 56

C Parameterization of the prototype model (4.8) 58

D Stability analysis of the prototype model (4.8) under state feedback . . . 61

E Rafael Kelly Award 66

References **66**

LIST OF FIGURES

2.1 Prototype sections description. 8

2.2 Electronic diagram of the Copley Controls 432 power amplifier. 8

2.3 Laboratory prototype (notation from Fig. 2.1). 9

2.4 Flowchart of the experimental setup. 10

3.1 Mechanical system acting forces in Section 1 of the prototype. 12

3.2 Servomotor model blocks diagram (see [1]). 13

3.3 MD1 and servomotor mounting. 13

3.4 Filtering. 17

3.5 Reference signal q_{r1} used for $\hat{a}$ and $\hat{b}$ estimation. 19

3.6 Reference signal q_{r2} used for $\hat{c}$ and $\hat{d}$ estimation. 21

3.7 Reference generator. 25

3.8 MATLAB real-time experiment diagram for implementing the tracking control law (3.33). 25

3.9 Performance of the persistence of excitation condition for the regressor (3.22). 26

3.10 Estimates $\hat{a}$ and $\hat{b}$ obtained through the ARIM. 28

3.11 Estimates $\hat{c}$ and $\hat{d}$ obtained through the ARIM. 28

3.12 FSIM tracking performance. 29

3.13 ARIM tracking performance. 29

3.14 $MD1$ and $W1$ devices. 30

3.15 ARIM tracking performance with 0.7V excitation applied to $MD1$ and clutch $C1$ disengaged. 31

4.1 Mechanical system acting forces along the whole prototype. 34

4.2 Section 2 of the prototype. 35

4.3 Parallel PD controller (4.32) used for stabilizing the model (4.8). 42

4.4 Simulation response of the prototype stabilized through the controller (4.32). 43

4.5 Reference signal q_{rf1} used for $\hat{a}_m$, $\hat{b}_m$, $\hat{g}_m$, $\hat{a}_s$ and $\hat{g}_s$ estimation. 44

4.6 Reference signal q_{rf2} used for $\hat{c}_m$, $\hat{d}_m$ and $\hat{c}_s$ estimation. 45

4.7 Estimates $\hat{a}_m$, $\hat{b}_m$, $\hat{c}_m$ and $\hat{d}_m$ obtained through the modified ARIM. . . . 46

4.8 Estimates $\hat{g}_m$, $\hat{a}_s$, $\hat{g}_s$ and $\hat{c}_s$ obtained through the modified ARIM. 47

4.9 Performance of the Persistence of Excitation condition (4.19) for the regressor (4.18a). 48

4.10 Performance of the Persistence of Excitation condition (4.19) for the regressor (4.18b). 48

1 WonderBox current response. 55

2 Magnetorheological damper torque as a function of the current. 55

3 Rafael Kelly Acknowledgment 66

LIST OF TABLES

2.1 Power amplifier configuration. 9

3.1 Notation used in Fig. 3.2. 13

3.2 Parameter identification results. 26

3.3 Results of ARIM with nominal inertia for several voltage values applied to the Wonder Box $W1$. 31

3.4 Results of ARIM with inertia $J2$ added, for several voltage values applied to the Wonder Box $W1$. 31

4.1 Parameters estimates obtained when the Section 1 and the Section 2 of the prototype work together. 45

CHAPTER 1

INTRODUCTION

Nowadays, DC servomechanisms are widely chosen over other options for robotics, control and automation, due to its low cost in comparison with alternative technologies, its low energy consumption, and because they are easy to control and there exist numerous controller developed by the manufacturers that are specifically devoted to handle these devices. Because of the above, the development of industrial applications is strongly connected to the improvement of the control of DC servomechanisms, focused on position and speed, so that the parameter identification takes an important place as a mean to design highly-precise control laws, able to follow complexes motion paths and keeping the tracking error as close to zero as possible.

The parameter identification of a servomechanism has been a subject of study repeatedly reported in the literature [1], [2], [3] and permit the development of model-based control laws [4], [5], [6], [7]. In the aforementioned works the identification focuses in systems showing a rigid coupling between the servomechanism and the load, i.e. these aproaches do not take into account flexibility. However, if the coupling is not rigid enough, then some resonance effects could occur considerably affecting the performance of the servomechanism [8].

Literature on parameter identification of servomechanisms considering flexibility is not abundant compared with the number of works where flexibility is ignored. The following is a brief literature review on this subject. The reference [9] proposes the identification of a servomechanism that drives a two-mass system, where the parameter identification is performed in open-loop and closed-loop. The reference [10] uses the Welch method that works in the frequency domain and utilizes an open-loop scheme. The methods described in [11] and [12] employs the discrete-time model of a two-mass mechanical system and the identification is carried out using open-loop and closed-loop schemes. In the reference [13] the flexibility of the system is produced by a belt drive transmission mechanism and the identification is achieved by means of a frequency based method applied to a discrete-time model.

The magnetorheological dampers are devices frequently used to reduce vibrations in electromechanical systems and are commonly applied to robot manipulators [14], [15], servodrives [16], actuators [17], [18], [19], [20], and haptic interfaces [21], [22], among others. In order to introduce damping, these dampers are filled with a liquid containing magnetic particles, and one or several coils mounted inside the damper allow applying a magnetic filed to the liquid. The coils are excited through an electric current produced by a power amplifier fed by a voltage signal. Increasing this signal also increases the current and the coils magnetic field, which in turn raises the viscosity of the liquid and consequently the mechanical damping that the damper delivers. The fact that it is easy to modulate the viscosity of magentorheological dampers through an electric signal has been exploited for vibration attenuation [23], for vibration control in cars [24], for producing variable compliance in humanoid locomotion systems [18], for seismic response reduction [25], for developing haptic interfaces [21], [22], for designing improved prosthesis [26], among many others areas.

A review on modeling and parameter identification of magnetorheological dampers [27] shows that these devices may exhibit a complex nonlinear behavior that

may be described through simple models including the Bingham model [28], or dynamic models like the Bouc-Wen or the Dahl models that include the hysteretic behavior of the magnetorheological damper [29]. Even if dynamic models accurately match experimental data compared with simple static models, they are more difficult to identify and in some cases this complexity would not be required.

Main objectives

The closed-loop parameter identification of the model of a rotational servomechanism for three different cases:

(1) A mechanical system composed by a servomechanism coupled to an inertial load and to an unexcited MD.

(2) A mechanical system composed by a servomechanism coupled to an inertial load and to an MD excited through different voltages.

(3) A mechanical system composed by a servomechanism coupled to an inertial load, to an unexcited MD and, to a second inertial load by means of a spring.

Particular objectives

The particular objectives along this work are the following:

(a) To apply a parameterization for the model that corresponds to the first and second cases.

(b) To develop a suitable parameterization for the model used in the third case.

(c) To propose a controller able to stabilize the system without previous knowledge on its parameters.

(d) To apply on-line and off-line Least Square algorithms to estimate the parameters of the systems mentioned before using the parameterizations previously obtained.

(e) To evaluate the identification schemes proposed through numeric simulation and real-time experiments carried out in a laboratory prototype.

The outline of the thesis is the following.

The Chapter 2 gives a complete description of the laboratory prototype used in the real-time experiments carried out in this work.

The Chapter 3 presents two parameter identification methods based on simple dynamic models of a servomechanism driving an inertial load with and without engaging a magnetorheological damper, which are applied to the laboratory prototype described in the Chapter 2 without considering the flexibility stage. The first method is the off-line State Filters Identification Method (SFIM) and generates a regressor vector through the use of linear state filters and only considers a model with viscous friction. The second method resorts on algebraic techniques for generating the regressor vector and an on-line Least Square algorithm, and the corresponding model takes into account viscous, Coulomb friction and constant disturbances. This method is termed as the Algebraic Recursive Identification Method (ARIM). Moreover, the chapter also presents the outcomes of some experiments where the magnetorheological damper attached to the servomechanism shaft is excited with several different voltages.

The Chapter 4 describes a modification that is applied to the ARIM presented in Chapter 3 in order to identify the parameters of the whole system, which corresponds to the third mentioned in the main objectives, i.e. when including the flexibility stage.

The Chapter 5 gives a complete review about this work, the main issues of each one of the chapters and the results obtained throughout the simulations and the real-time experiments. The conclusions derive of the aforementioned reviews also stand in this chapter.

It is worth noting that the paper:

"Juan Manuel Martin del Campo, Rubén Garrido. Parameter identification of a servomotor equipped with a magnetorheological damper. Memorias del XVIII Congreso Mexicano de Robótica COMROB XIX. Mazatlán, Sinaloa, 8 al 10 de Noviembre (2017): 247-252."

derived from this work received the *Rafael Kelly Award* for the best postgraduated student paper. A copy of the award is shown in Appendix E.

CHAPTER 2

EXPERIMENTAL SETUP

The prototype used in all the experiments is composed of two sections as shown in Fig. 2.1 and Fig. 2.3. Section 1 of the prototype consists of a servomotor Moog model C34-L80-W40 [30], driven by a power amplifier Copley Controls model 432 [31], working in current mode. Fig. 2.2 depicts the electronic diagram of the power amplifier and Table 2.1 shows its configuration values.

An optical encoder model ST50 (E1) and its complementary tachometer model SA-7388F-1 with 1024 PPR (Pulses Per Revolution), both from ServoTek [32], measure the angular position and the angular velocity of the servomotor, respectively. A magnetorheological rotary brake Lord (MD1) model MRB-2107-3 [33], is coupled directly to the motor shaft, and a *WonderBox controller* (W1) Lord [34], driven by a voltage signal in the *0V - 5V* range, controls the current applied to the MD1. The inertia $J1$ is fixed to the motor shaft, and the clutch 1 (C1) OGURA, model OPC20 EM Magnetic Particle Clutch [35], allows adding an extra inertia $J2$ to the servomotor.

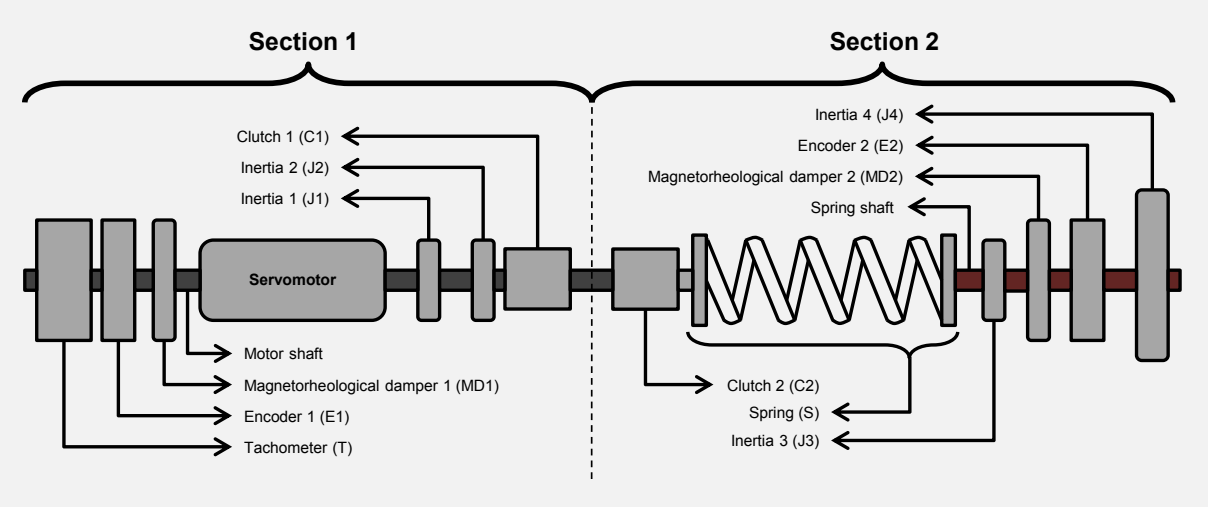

Figure 2.1: Prototype sections description.

On the other hand, Section 2 of the prototype consists of a spring and a magnetorheological rotary brake (MD2) similar to the MD1 and also controlled by a *WonderBox controller* (W2), that accomplishes the task of applying magnetorheological damping to the spring shaft (see Fig. 2.1).

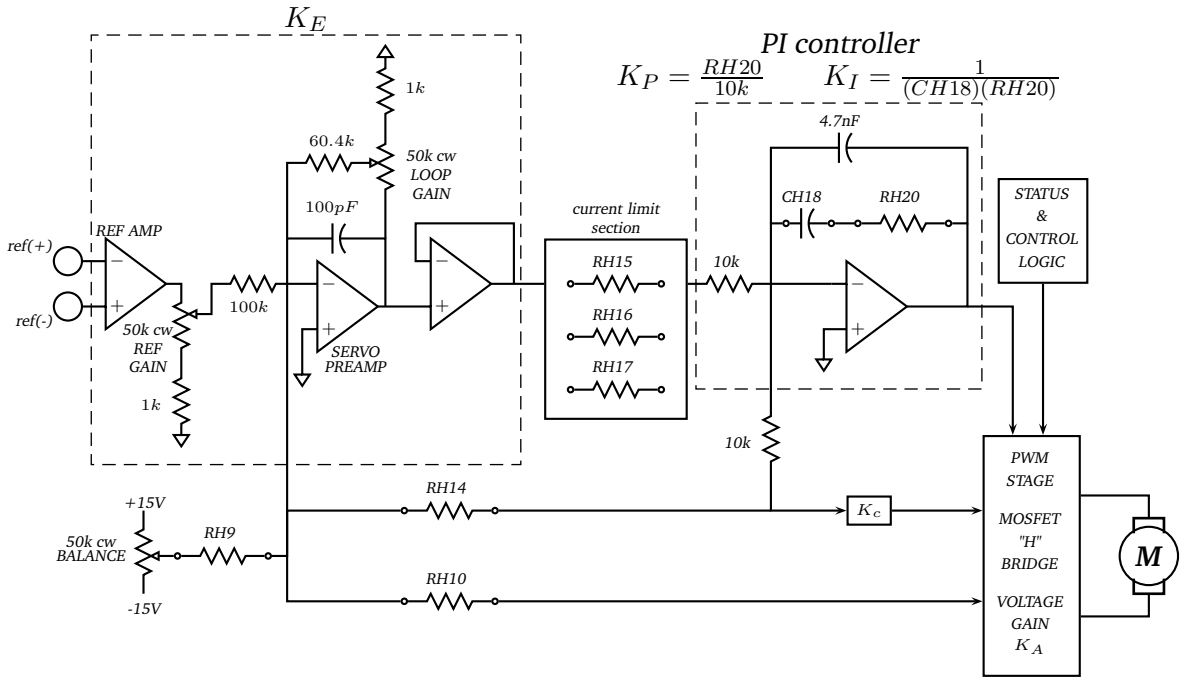

Figure 2.2: Electronic diagram of the Copley Controls 432 power amplifier.

Part	Function	Value	Units
RH9	Balance/Test	10	$M\Omega$
RH10	Output voltage feedback	$open$	Ω
RH14	IR compensation feedback	$open$	Ω
RH15	Peak current limit	15	$k\Omega$
RH16	Continuous current limit	15	$k\Omega$
RH17	Peak time-limit	330	$k\Omega$
CH18	Load inductance compensation	4.7	nF
RH20	Load inductance compensation	40.2	$k\Omega$

Table 2.1: Power amplifier configuration.

An optical encoder USDigital (E2), model 2500-500-IE-H-D-B [36] with 2500 PPR, measures the angular position of the spring shaft to which the inertia $J3$ is fixed. Inertia $J4$ is also fixed to the spring shaft, however, it can be whether replaced or removed manually. Another OGURA clutch (C2) enables coupling of Section 1 and Section 2 of the prototype. Therefore, the servomotor also drives inertia $J3$ and $J4$ through the spring S (see Fig. 2.3).

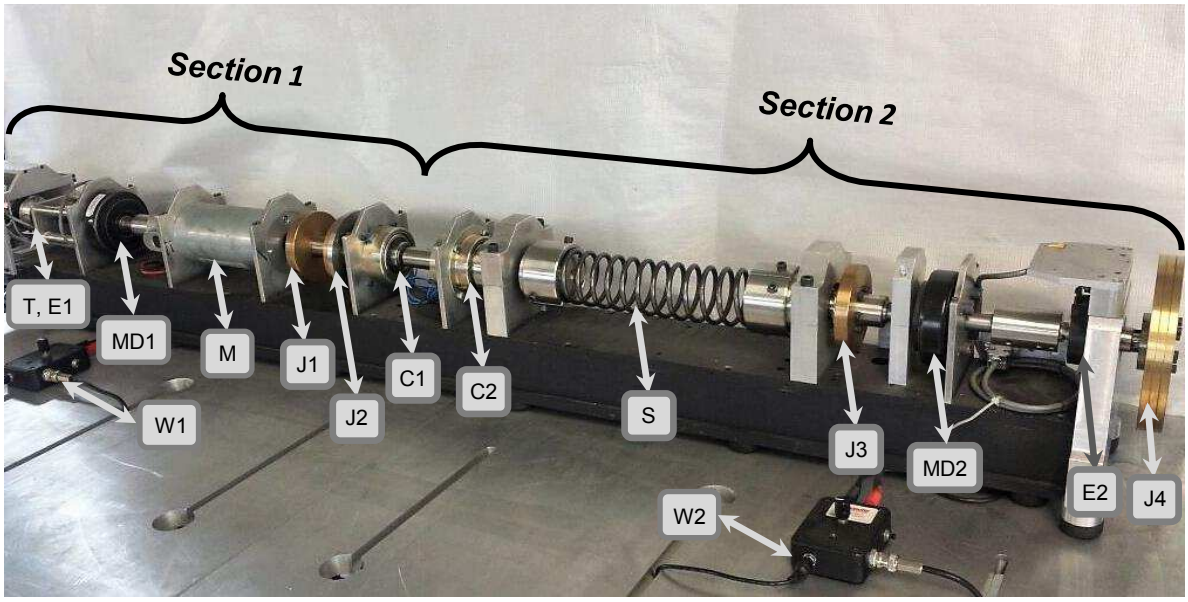

Figure 2.3: Laboratory prototype (notation from Fig. 2.1).

Algorithms and simulations run in a 32-bits PC Intel Core 2 Quad, over the Windows 7 Professional operating system using *Simulink-MATLAB R2011b*. *QUARC 2.2.1* software [37] and a *Q8 Data Acquisition Board* [38] inside the computer, both from Quanser, consult data acquisition by means of the *Quanser Terminal Board* and allow communication between the prototype and the coded algorithms (see Fig. 2.4).

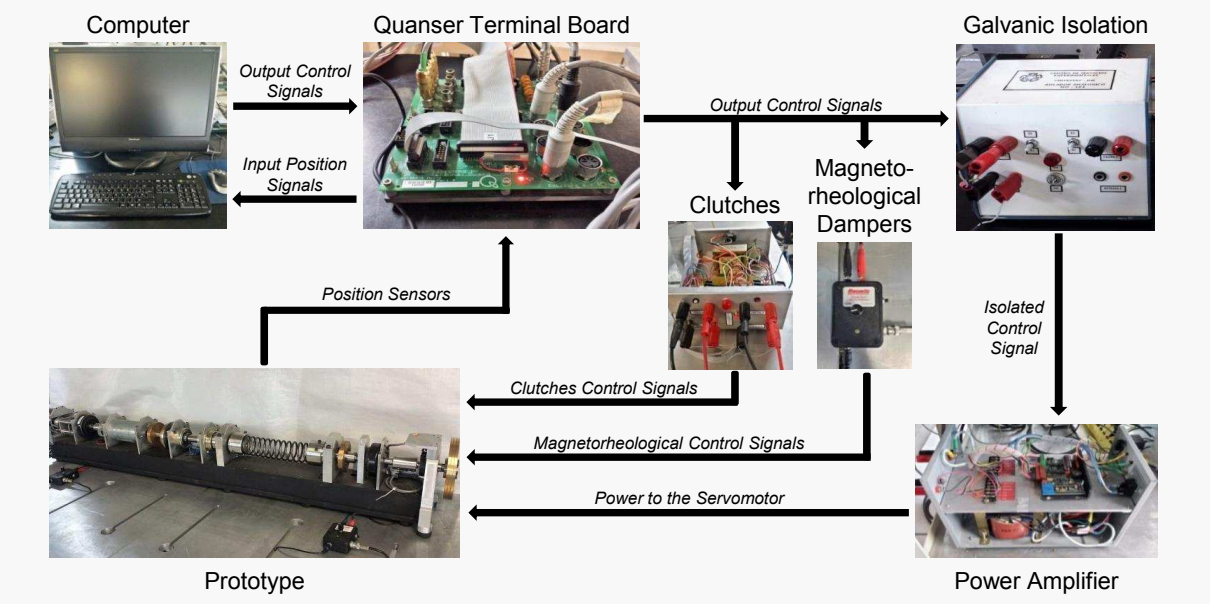

Figure 2.4: Flowchart of the experimental setup.

CHAPTER 3

PARAMETER IDENTIFICATION OF THE PROTOTYPE WITHOUT CONSIDERING FLEXIBILITY

3.1 Prototype Section 1 model

This chapter is devoted to the parameter identification of Section 1 of the prototype. In this case the clutch $C2$ remains disengaged thus precluding the contribution of Section 2, which includes the spring S to the dynamics of Section 1. As mentioned is Chapter 2, Section 1 of the prototype consists of a power amplifier, the magnetorheological damper $MD1$, a servomotor, the inertia $J1$, the inertia $J2$ and the clutch $C1$.

The 2nd Newton's law [39] states that external and internal torques acting on a rotational system must kept in balance. Thereby, Fig. 3.1 shows the acting torques on the Section 1 of the prototype. Note that clutches $C1$ and $C2$ remain disengaged.

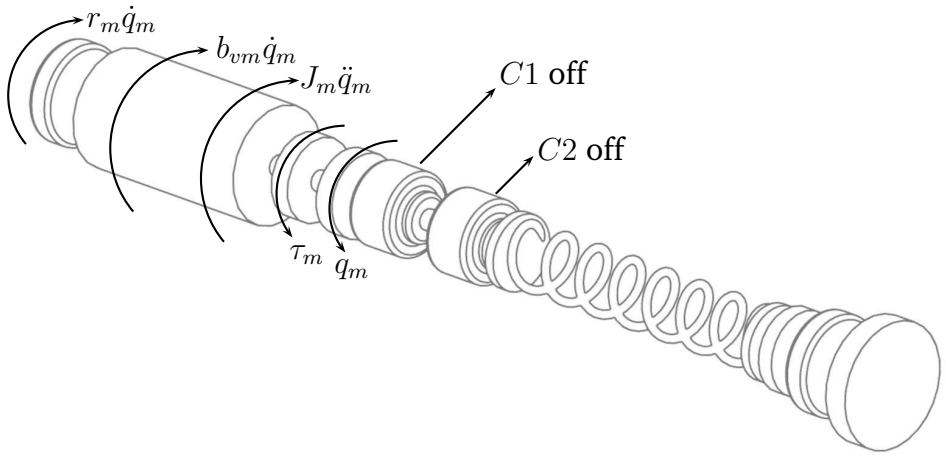

Figure 3.1: Mechanical system acting forces in Section 1 of the prototype.

On the other hand, the power amplifier works in current mode, so that the current loop (see Fig. 3.2) accomplishes the task of keeping the control voltage u proportional to the armature current I_a and consequently proportional to the electromagnetic torque τ_m (see [40]), i.e.

$$\tau_m = Ku(t) \tag{3.1}$$

Fig. 3.2 depicts the block diagram of the power amplifier configured in current mode, the DC servomotor and the position sensor $E1$. Inertia J_m is the sum of the servomotor inertia J_{ser}, the brass disk inertia $J1$ and the encoder inertia J_e. Due to the high integral gain K_I of the power amplifier, the electrical time constant is much smaller that the mechanical time constant. Therefore, the power amplifier dynamics are subsequently ignored. The above simplification, Newton's second law and Fig. 3.1 permit obtaining the following model of the prototype Section 1

$$J_m\ddot{q}_m(t) + f\left(\dot{q}_m(t)\right) = \tau_m + \tau_d \tag{3.2}$$

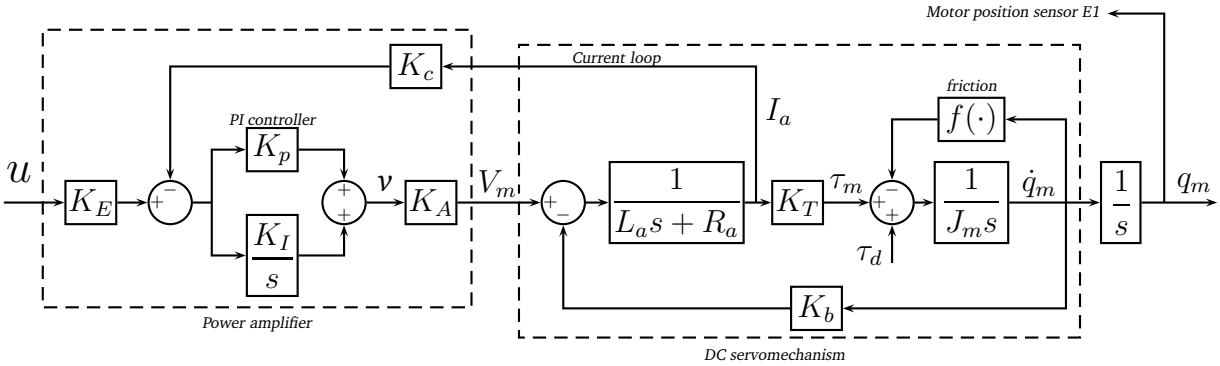

Figure 3.2: Servomotor model blocks diagram (see [1]).

Block diagram description			
K_E	Amplifier input gain	K_p	Proportional gain
K_I	Integral gain	K_c	Current loop gain
K_A	Power amplifier gain	V_m	Servomotor input voltage
R_a	Armature resistance	L_a	Armature inductance
K_T	Torque constant	K_b	Back EMF constant
J_m	Section 1 inertia	τ_d	Amplifier parasitic disturbances
q_m	Servomotor angular position	$\dot{q}_m$	Servomotor angular velocity
$f(\cdot)$	Friction torques		

Table 3.1: Notation used in Fig. 3.2.

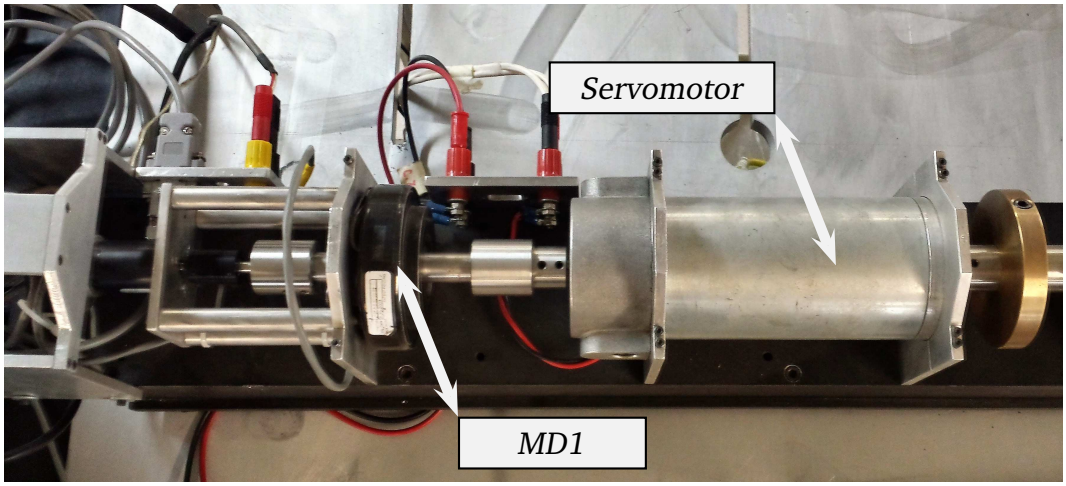

Figure 3.3: MD1 and servomotor mounting.

The term $f\left(\dot{q}_m(t)\right)$ accounts for the servomotor and the magnetorheological damper friction. The Bingham model for a magnetorheological damper [27] is considered for describing the friction phenomena in the magnetorheological damper

$$f\left(\dot{q}(t)\right) = f_m \dot{q}_m(t) + \mu_m \text{sign}\left(\dot{q}_m(t)\right) \tag{3.3}$$

where the term $f_m = b_{vm} + r_m$ represents the motor viscous and the magnetorheological friction coefficients respectively, and the term μ_m represents the Coulomb friction coefficient. The sign$(\dot{q}_m(t))$ function is defined as

$$\text{sign}(\dot{q}_m(t)) = \begin{cases} 1, & \text{if} \quad \dot{q}_m(t) > 0 \\ 0, & \text{if} \quad \dot{q}_m(t) = 0 \\ -1, & \text{if} \quad \dot{q}_m(t) < 0 \end{cases} \tag{3.4}$$

Substituting equations (3.1) and (3.3) into equation (3.2) yields

$$J_m \ddot{q}_m(t) + f_m \dot{q}_m(t) + \mu_m \text{sign}\left(\dot{q}_m(t)\right) = K u(t) + \tau_d \tag{3.5}$$

which has the following alternative writing

$$\ddot{q}_m(t) = -a\dot{q}_m(t) + b u(t) - c\text{sign}\left(\dot{q}_m(t)\right) + d \tag{3.6}$$

where the next definitions are used

$$a = \frac{f_m}{J_m}; \quad b = \frac{K}{J_m}; \quad c = \frac{\mu_m}{J_m}; \quad d = \frac{\tau_d}{J_m}; \quad K = \frac{K_E K_T}{K_c}$$

3.2 Parameter identification

The Filter State Identification [41] (FSIM) and the Algebraic Recursive Identification [1] (ARIM) methods furnish a way to estimate the parameters of the servomechanism model (3.6). So as to apply the two identification methods described in the followings sections, it is necessary to stabilize the Section 1 of the prototype through the next Proportional Derivative (PD) controller

$$\begin{aligned} u(t) &= K_p \left[q_r(t) - q_m(t)\right] - K_d \dot{q}_e(t) \\ \dot{q}_e(t) &= \gamma \left[q_m(t) - q_e(t)\right] \end{aligned} \tag{3.7}$$

Constants K_p and K_d correspond to the proportional and integral gains of the controller, $q_r(t)$ is a reference used for identification purposes, $\dot{q}_e(t)$ is an estimate of the servomotor angular velocity $\dot{q}_m(t)$, and γ is a positive constant.

3.2.1 Filter State Identification Method (FSIM)

This method uses a simplified version of the model (3.6) without considering the Coulomb friction and the disturbances terms, i.e.

$$\ddot{q}_m(t) = -a\dot{q}_m(t) + bu(t) \tag{3.8}$$

Note that the only measurement available corresponds to the servomotor angular position q_m. Consequently it is not possible to produce a linear regression from model (3.8) to estimate the unknown parameters a and b since measurements of $\dot{q}_m$ and $\ddot{q}_m$ are not available. To circumvent this problem, a filtered version of the model (3.8) is obtained through linear state filters.

Applying the Laplace transform to (3.8) produces the next equality

$$s^2 Q_m(s) = -asQ_m(s) + bU(s) \tag{3.9}$$

where $Q(s) = \mathcal{L}\{q_m(t)\}$, $U(s) = \mathcal{L}\{u(t)\}$, and the operator $\mathcal{L}\{\cdot\}$ corresponds to the Laplace transform operator. Next, define the filter

$$F(s) = \frac{f_2}{s^2 + f_1 s + f_2} \tag{3.10}$$

where the terms f_1 and f_2 are positive constants. Multiplying both sides of (3.9) by $F(s)$ leads to the next equation

$$F(s)s^2 Q_m(s) = -aF(s)sQ_m(s) + bF(s)U(s) \tag{3.11}$$

The next variables

$$\begin{aligned} s^2 Q_f(s) &= F(s)s^2 Q_m(s) \\ sQ_f(s) &= F(s)sQ_m(s) \\ Q_f(s) &= F(s)Q_m(s) \\ U_f(s) &= F(s)U(s) \end{aligned} \tag{3.12}$$

allow writing (3.11) as follows

$$s^2 Q_f(s) = -asQ_f(s) + bU_f(s) \tag{3.13}$$

Finally, applying the inverse Laplace transform to (3.13) yields

$$\ddot{q}_f(t) = -a\dot{q}_f(t) + bu_f(t) \tag{3.14}$$

with $\ddot{q}_f(t) = \mathcal{L}^{-1}\{s^2 Q_f(s)\}$, $\dot{q}_f(t) = \mathcal{L}^{-1}\{sQ_f(s)\}$ and $u_f(t) = \mathcal{L}^{-1}\{U(s)\}$, which are the filtered versions of $\ddot{q}_m(t)$, $\dot{q}_m(t)$ and $u(t)$ respectively, and unlike to the model (3.8), $\ddot{q}_f(t)$ and $\dot{q}_f(t)$ are available by filtering the servomotor angular position $q_m(t)$

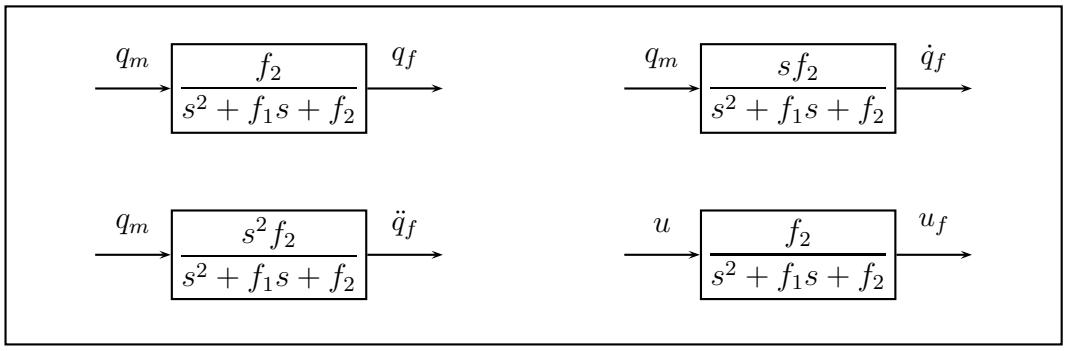

Figure 3.4: Filtering.

For applying the FSIM, the model (3.14) is written in the following regression form

$$\begin{aligned} z_L(t) &= \ddot{q}_f(t) \\ &= \phi_L(t)^T\theta_L \end{aligned} \tag{3.15}$$

$$\phi_L(t) = [-\dot{q}_f(t) \;\; u_f(t)]\,; \qquad \theta_L = [a \;\; b]^T$$

which is also valid at the time instants $t = T, 2T, \ldots, (K-1)T, KT, \ldots$ where T is a sampling time period. Therefore

$$z_L(K) = \phi_L(K)^T\theta_L \tag{3.16}$$

and the off-line Least Square algorithm is used to estimate θ_L. So as to apply this method, it is necessary to sample $z_L(K)$ and the regressor vector $\phi_L(K)$ along K time instants to build the following terms

$$A_L = \begin{bmatrix} \phi_L(1)^T \\ \phi_L(2)^T \\ \vdots \\ \phi_L(K-1)^T \\ \phi_L(K)^T \end{bmatrix}; \qquad Z_L = \begin{bmatrix} z_L(1) \\ z_L(2) \\ \vdots \\ z_L(K-1) \\ z_L(K) \end{bmatrix} \tag{3.17}$$

Hence, the estimate $\hat{\theta}_L$ of θ_L is given by the next expression [42]

$$\hat{\theta}_L = \left(A_L{}^T A_L\right)^{-1} A_L{}^T Z_L \tag{3.18}$$

Also, the system under identification must be excited by a signal with a wide frequency spectrum to achieve that input and output as well as its corresponding derivatives, change sufficiently in time. The conditioning κ gives a suitable way to know how good the excitation signal applied is and is defined as

$$\kappa = \frac{\lambda_{max}\left(A_L{}^T A_L\right)}{\lambda_{min}\left(A_L{}^T A_L\right)} \tag{3.19}$$

being $\lambda_{max}\left(A_L{}^T A_L\right)$ and $\lambda_{min}\left(A_L{}^T A_L\right)$ the largest and the smallest eigenvalues of the matrix $A_L{}^T A_L$, respectively. Conditioning values closer to 1 indicate an adequate excitation signal because both eigenvalues are about of the same magnitude order. A good choice for the signal excitation is filtered white noise, being careful of not applying it to the servomotor for extended periods of time in order to avoid permanent damages.

3.2.2 Algebraic Recursive Identification Method (ARIM)

This method is based on operational calculus techniques [43] and on a recursive Least Square algorithm (see [44] and [45]) applied to the model (3.6). According to [1], the method is divided into two steps. In the first step the ARIM uses signals q_m and u to estimate the parameters a and b from (3.6) that correspond to the linear part of the model.

The reference signal q_{r1} depicted in Fig. 3.5 is composed of a ramp an two sinusoids and fulfills the Persistence of Excitation (PE) condition [45]. It must be applied to the system under identification in the time interval $[0,\, t_0]$ to make the

servomotor rotate only in one direction and enforce the term sign$(\dot{q}_m)$ in the Coulomb friction to have a constant value. This fact allows writing (3.6) as follows

$$\ddot{q}_m(t) = -a\dot{q}_m(t) + bu(t) + \nu \tag{3.20}$$

where $\nu = -c_m \text{sign}\,(\dot{q}_m(t)) + d$. Note that

$$\nu = \begin{cases} -c_m + d, & \text{if} \quad \dot{q}_m(t) > 0 \\ c_m + d, & \text{if} \quad \dot{q}_m(t) < 0 \end{cases} \tag{3.21}$$

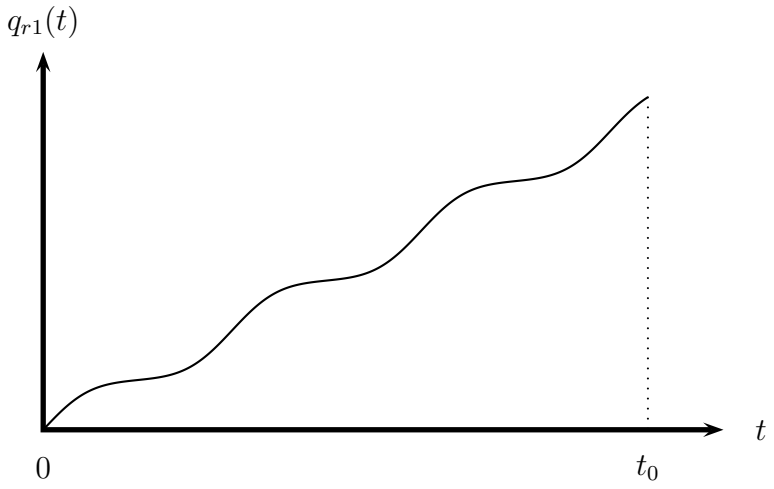

Figure 3.5: Reference signal q_{r1} used for $\hat{a}$ and $\hat{b}$ estimation.

The next regression model is obtained for (3.6) using the operational methodology

$$z_A(t) = {\theta_A}^T \phi_A(t) \tag{3.22}$$

$$\phi_A = [\phi_1(t) \;\; \phi_2(t)]^T; \qquad \theta_A = [a \;\; b]^T$$

where (see Appendix B)

$$z(t) = a\phi_1(t) + b\phi_2(t) \tag{3.23}$$

and

$$z(t) = t^3 q_m - 9\int t^2 q_m + 18\int^{(2)} t q_m - 6\int^{(3)} q_m$$
$$\phi_1(t) = -\int t^3 q_m + 6\int^{(2)} t^2 q_m - 6\int^{(3)} t q_m$$
$$\phi_2(t) = \int^{(2)} t^3 u - 3\int^{(3)} t^2 u$$

The operator $\int^{(n)} \rho(t)$ represents the iterated integral $\int_0^t \int_0^{\tau_1} \dots \int_0^{\tau_{n-1}} \rho(\tau_n) d\tau_n \dots d\tau_2 \tau_1$. It is worth pointing out that the regression model (3.22) does not contain the constant term *v* appearing in (3.20), and is also valid for the time instants $t = T, 2T, ..., (k-1)T, kT, ...$ where T is the sampling period, i.e.

$$z_A(kT) = {\theta_A}^T \phi_A(kT) \tag{3.24}$$

or simply

$$z_A(k) = {\theta_A}^T \phi_A(k) \tag{3.25}$$

The regression model (3.25) allows performing the standard Least Square algorithm (3.26) (see [44] and [45]) where the term $\hat{\theta}_A$ is an estimated of θ_A, P is the covariance gain matrix and ϵ is the estimation error.

$$\begin{aligned}
\hat{\theta_A}(k) &= \hat{\theta}_A(k-1) + L(k)\epsilon(k) \\
L(k) &= \frac{P(k-1)\phi_A(k)}{1 + {\phi_A}^T(k)P(k-1)\phi_A(k)} \\
P(k) &= P(k-1) + \frac{P(k-1)\phi_A(k){\phi_A}^T(k)P(k-1)}{1 + {\phi_A}^T(k)P(k-1)\phi_A(k)} \\
\epsilon(k) &= z_A(k) - {\phi_A}^T(k)\hat{\theta_A}(k-1)
\end{aligned} \tag{3.26}$$

Moreover, the vector $\phi_A(k)$ satisfies the Persistence of Excitation condition [45] if

$$\lim_{k\to\infty} \Omega_k = \lim_{k\to\infty} \lambda_{min} \left[\sum_{j=1}^{k} A_A(j)\right] = \infty \tag{3.27}$$

where

$$A_A(j) = \phi_A(j)\phi_A^T(j) \tag{3.28}$$

and $\lambda_{min}[\cdot]$ is the smallest eigenvalue operator. In the second step of identification the estimates $\hat{c}$ and $\hat{d}$ are computed using the reference signal (3.29) shown in Fig. 3.6 in the time interval $[t_0,\, t_f]$

$$q_{r2} = \begin{cases} m(t-t_0) + q_{r1}(t_0), & \text{if} \quad t \in [t_0,\, t_0+\delta] \\ \\ -m\,[t-(t_0+2\delta)] + q_{r1}(t_0), & \text{if} \quad t \in [t_0+\delta,\, t_f] \end{cases} \tag{3.29}$$

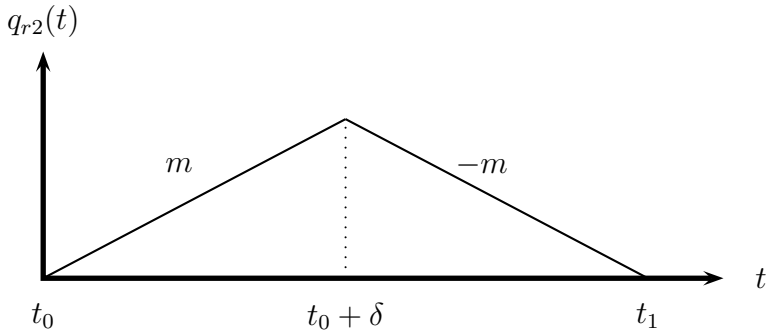

Figure 3.6: Reference signal q_{r2} used for $\hat{c}$ and $\hat{d}$ estimation.

The terms $m > 0$ and $-m < 0$ correspond to the slopes of the reference $q_r(t)$ and $\delta = (t_f - t_0)/2$. Thus, the following set of conditions hold at the end of the time interval $t \in [t_0,\, t_0+\delta]$ and $t \in [t_0+\delta,\, t_0]$, respectively

$$\left.\begin{aligned} \dot{q}_m(t) &= m \\ \text{sign}(\dot{q}_m(t)) &= 1 \\ \ddot{q}_m(t) &= 0 \\ u(t) &= u_+ \end{aligned}\right\} \quad t \in [t_0,\, t_0+\delta]$$

$$\left.\begin{aligned} \dot{q}_m(t) &= -m \\ \text{sign}(\dot{q}_m(t)) &= -1 \\ \ddot{q}_m(t) &= 0 \\ u(t) &= u_- \end{aligned}\right\} \quad t \in [t_0+\delta,\, t_0]$$

using each one of the above set of conditions, model (3.6) becomes

$$c - d = -am + bu_+ \tag{3.30a}$$

$$-c - d = am + bu_- \tag{3.30b}$$

The corresponding estimated model for (3.30) is

$$\hat{c} - \hat{d} = -\hat{a}m + \hat{b}u_+ \tag{3.31a}$$

$$-\hat{c} - \hat{d} = \hat{a}m + \hat{b}u_- \tag{3.31b}$$

A mistake was found in solving of the set of equations (3.31) for $\hat{c}$ and $\hat{d}$ in [1], whose amendment remains

$$\hat{c} = -\hat{a}m + \hat{b}u_+ + \hat{d} \tag{3.32a}$$

$$\hat{d} = -\frac{\hat{b}\,[u_+ + u_-]}{2} \tag{3.32b}$$

3.3 Experimental comparison between the FSIM and the ARIM algortihms

In order to perform parameter identification using both methods the servomotor is controlled using the PD algorithm (3.7) tuned according to $K_p = 20$, $K_d = 0.46$, $\gamma = 300$ and implemented using a sampling time of $0.001\,s$.

In the case of FSIM, the exciting signal is produced through the *band-limited White noise* block from Simulink with a noise power of 0.02 and a sampling time of $100\,ms$. The coefficients of the filters shown in Fig. 3.4 are set to $f_1 = 40$ and $f_2 = 400$. Finally, the parameter estimates are found by solving equation (3.18). On the other hand, the ARIM employs the signal $q_{r1} = 11t + 4\sin(0.8\pi t) + 0.25\sin(1.6\pi t)$ with $t_0 = 10\,s$, i.e.,

in the time interval $[0\,s,\ 10\,s]$. Moreover, the solver ODE1-Euler with a fixed step size of $0.001\,s$ is used for implementing the regressor (3.22). The signal q_{r2} depicted in Fig. 3.6 is applied as reference for the PD controller (3.7) with $t_f = 20\,s$, i.e., during the time interval $[10\,s,\ 20\,s]$. The covariance gain matrix and the initial estimated values are $P(0) = \text{diag}[10\,000,\ 10\,000]$ and $\theta(0) = [0,\ 0]^T$, correspondingly.

The pertinence of the estimates obtained through both algorithms is evaluated by means of solving the tracking control problem described in the next section.

3.3.1 Model validation

In order to validate the identified parameters through the FSIM and the ARIM algorithms, they are used for solving a trajectory tracking control problem by means of applying the next control law to the Section 1 of the prototype

$$u(t) = \frac{1}{\hat{b}}\left[\alpha_2 e(t) + \alpha_1 \dot{e}(t) + \ddot{q}_r(t) + \hat{a}\dot{q}_m(t) + \hat{c}\,\text{sign}\left(\dot{q}_m(t)\right) - \hat{d}\right] \tag{3.33}$$

Adding and subtracting $\hat{b}u(t)$ to $\ddot{e}(t) = \ddot{q}_r(t) - \ddot{q}_m(t)$ leads to

$$\ddot{e}(t) = \ddot{q}_r(t) - \ddot{q}_m(t) + \hat{b}u(t) - \hat{b}u(t) \tag{3.34}$$

Replacing (3.6) in (3.34) yields the next error dynamics

$$\ddot{e}(t) + \alpha_1 \dot{e}(t) + \alpha_2 e(t) = \Phi\psi \tag{3.35}$$

$$\Phi = \begin{bmatrix}\hat{a} - a & \hat{b} - b & \hat{c} - c & \hat{d} - d\end{bmatrix}$$
$$\psi = [-\dot{q}_m(t)\ \ u(t)\ \ -\,\text{sign}(\dot{q}_m(t))\ \ 1]^T$$

When the equation (3.35) is homogeneous the error dynamic tends to zero as long as the real part of the roots of the characteristic polynomial associated to (3.35) lie in the left half plane [46]. The characteristic polynomial of (3.35) is

$$\begin{aligned} s^2 + \alpha_1 s + \alpha_2 &= 0 \\ (s + p_1)(s + p_2) &= 0 \end{aligned} \tag{3.36}$$

where

$$\begin{aligned} \alpha_1 &= p_1 + p_2 \\ \alpha_2 &= p_1 p_2 \end{aligned} \tag{3.37}$$

and $-p_1$, $-p_2$ are the roots of (3.35). According to the Ruth-Hurwitz criterion [47] the aforementioned condition ($Re(p_1), Re(p_2) > 0$) is fulfilled for equation (3.35) if and only if both coefficients α_1 and α_2 are positives. There are two possible cases when the right-hand side of equation (3.35) is equal to zero. The first one occurs when the vector Φ and the vector ψ are orthogonal; i.e.

$$-\tilde{a}\dot{q}_m(t) + \tilde{b}u(t) - \tilde{c}\text{sign}(\dot{q}_m(t)) + \tilde{d} = 0 \tag{3.38}$$

however, this condition does not happen during the experiments. For its part, the second case occurs when the identified parameters are equal to the servomechanism parameters. Note that the control law (3.33) seeks to cancel out the terms $a\dot{q}_m(t)$, $c\text{sign}(\dot{q}_m(t))$, d and to compensate the input gain b. Hence, the tracking error converges to a neighborhood of zero as long as the parameters estimated are close to the real parameters.

$$\left.\begin{aligned} \hat{a} - a &\approx 0 \\ \hat{b} - b &\approx 0 \\ \hat{c} - c &\approx 0 \\ \hat{d} - d &\approx 0 \end{aligned}\right\} \quad \Rightarrow \quad -\tilde{a}\dot{q}_m(t) + \tilde{b}u(t) - \tilde{c}\text{sign}(\dot{q}_m(t)) + \tilde{d} \approx 0 \tag{3.39}$$

For implementing the tracking control law (3.33) the reference signal has to be available as well as its first and second time derivative, which are generated by means of the filter shown in Fig. 3.7, where the terms r, q_r, $\dot{q}_r$ and $\ddot{q}_r$ represent the original reference signal, the reference position, the reference velocity and the reference acceleration.

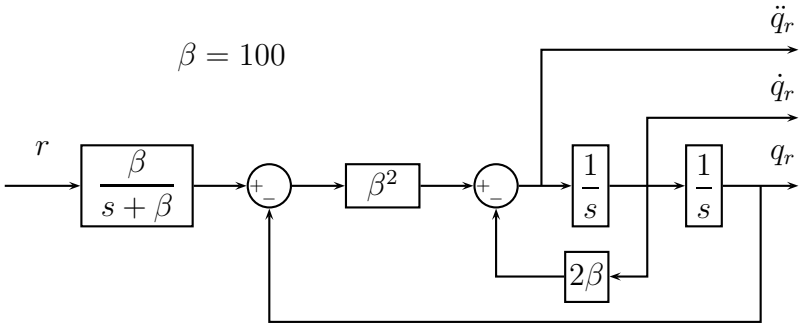

Figure 3.7: Reference generator.

The desired poles of the error dynamics (3.35) are placed at $p_1 = 6$ and $p_2 = 6$, so that $\alpha_1 = 12$ and $\alpha_2 = 36$, and (3.35) satisfies the Routh- Hurwitz stability criterion. The next MATLAB-Simulink diagram is implemented for computing the trajectory tracking control problem that is used for assessing the pertinence of the parameters estimates

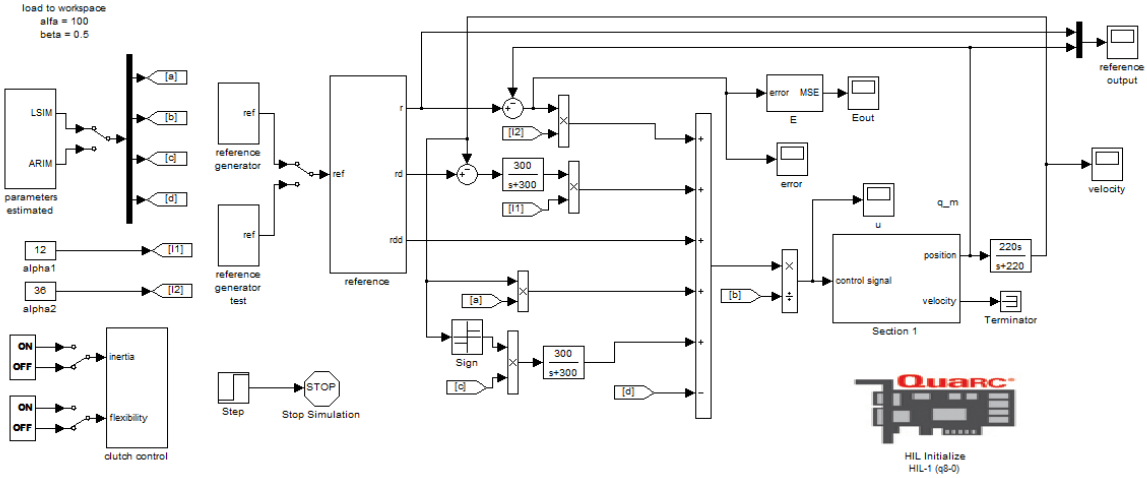

Figure 3.8: MATLAB real-time experiment diagram for implementing the tracking control law (3.33).

The squared error E serves as a measure of the tracking performance and is computed as follows

$$E = \int_{t_{in}}^{t_a} e(t)^2 \tag{3.40}$$

with $e(t) = q_r(t) - q_m(t)$, $t_{in} = 2\,s$, $t_a = 20\,s$ and a sampling period of $0.001\,s$.

3.3.2 Experimental results

Table 3.2 resumes the experimental results of the parameter identification and the performance of the model validation for both algorithms. Furthermore, the value of the conditioning κ for the FSIM algorithm is 78.0491 which indicates that the excitation signal chosen for identification of the linear part of the model (3.6) is adequate.

Identification	W1	Parameter identification				Performance
Method	Voltage (V)	$\hat{a}$	$\hat{b}$	$\hat{c}$	$\hat{d}$	E
FSIM	0	5.1791	163.7599	-	-	23 504.00
ARIM	0	0.4580	170.9007	13.0808	1.8532	26.32

Table 3.2: Parameter identification results.

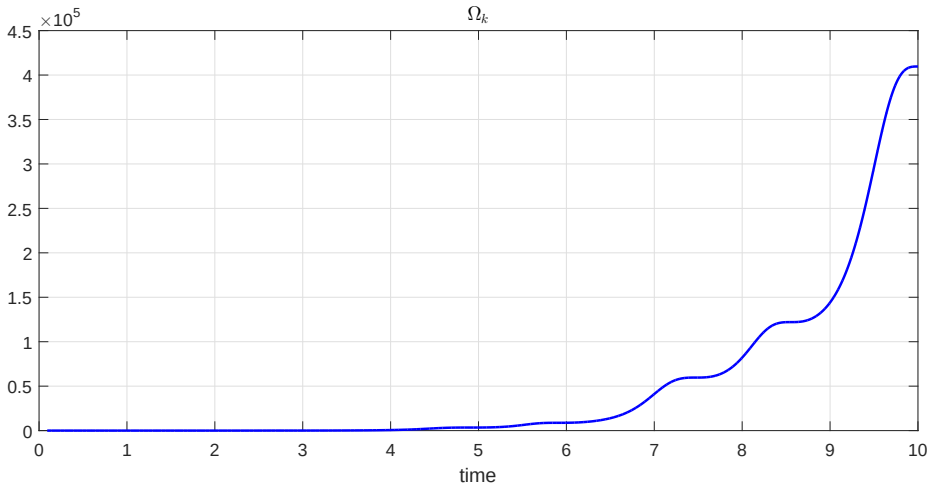

Figure 3.9: Performance of the persistence of excitation condition for the regressor (3.22).

Fig. 3.9 evidences that the value of Ω_k (3.27) tends to infinity when $k \to \infty$ thus excitation signal in Fig. 3.5 and 3.6 satisfy the Persistence of Excitation condition. Fig. 3.10 and Fig. 3.11 show the parameters estimated through the ARIM. The angular displacement measurements of the motor shaft are given in revolutions (r).

Note also that a slight difference exists between parameters $\hat{a}$ and $\hat{b}$ obtained by means of the FSIM and the ARIM algorithms. The experimental results show that the FSIM could be affected by the contributions of Coulomb friction and constant disturbances not considered in the model (3.14). An proper interpretation of this behavior is the following. The system damping represented by the parameter a increases in the FSIM algorithm to compensate for the absence of the Coulomb friction coefficient c that is not considered in (3.14), whereas the input gain represented by the parameter b decreases to compensate the constant disturbances d present in the dynamics (3.2) and also not considered in (3.14). The parameters estimated through the FSIM produce a large squared error E value compared with the value of E produced using the parameters provided by the ARIM. The above is observed in the tracking experiments results depicted in Fig. 3.12 and 3.13. An explanation for these outcomes is again the fact that the identification model (3.14) used in the FSIM does not consider Coulomb friction and constant disturbances whereas model (3.6) used in the ARIM does consider contributions of these terms.

The FSIM algorithm could be accurate enough when the identified servomechanism does not exhibit high Coulomb friction and constant disturbances levels because the error produced by these terms can be efficiently counteracted through a uncertainty observer [48] or the integral action of a Proportional Integral Derivative (PID) [49]. The FSIM algorithm is easily computed thanks to the components of the regressor vector $\phi_L(t) = [-\dot{q}_f(t) \;\; u_f(t)]$ are obtained by means of filtering the direct measurements of $q(t)$ and $u(t)$ from the prototype. Moreover, the system under identification is excited with a common low-amplitude white noise generator.

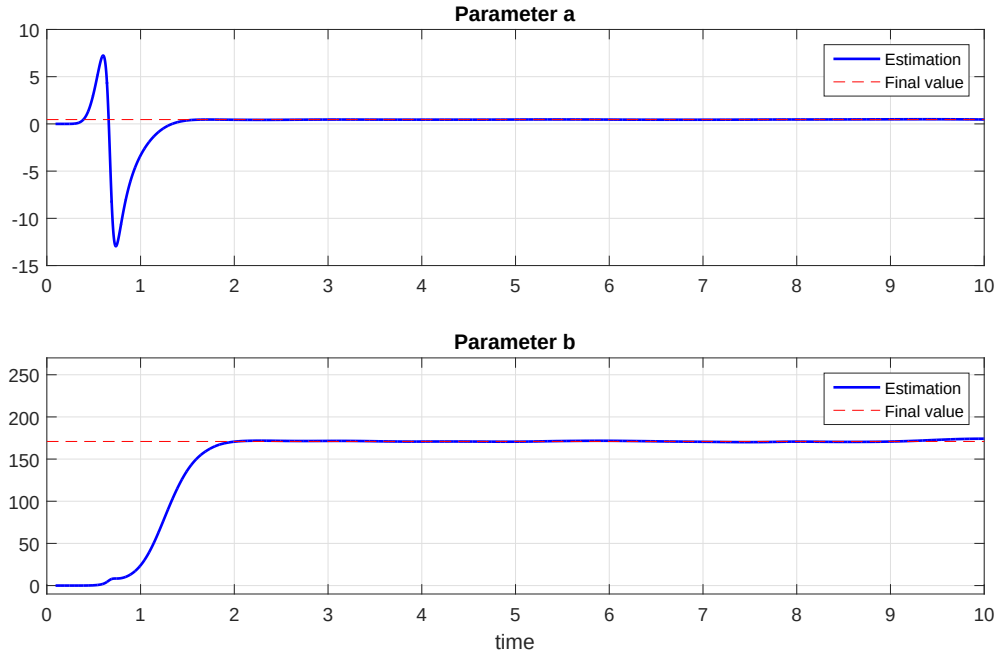

Figure 3.10: Estimates $\hat{a}$ and $\hat{b}$ obtained through the ARIM.

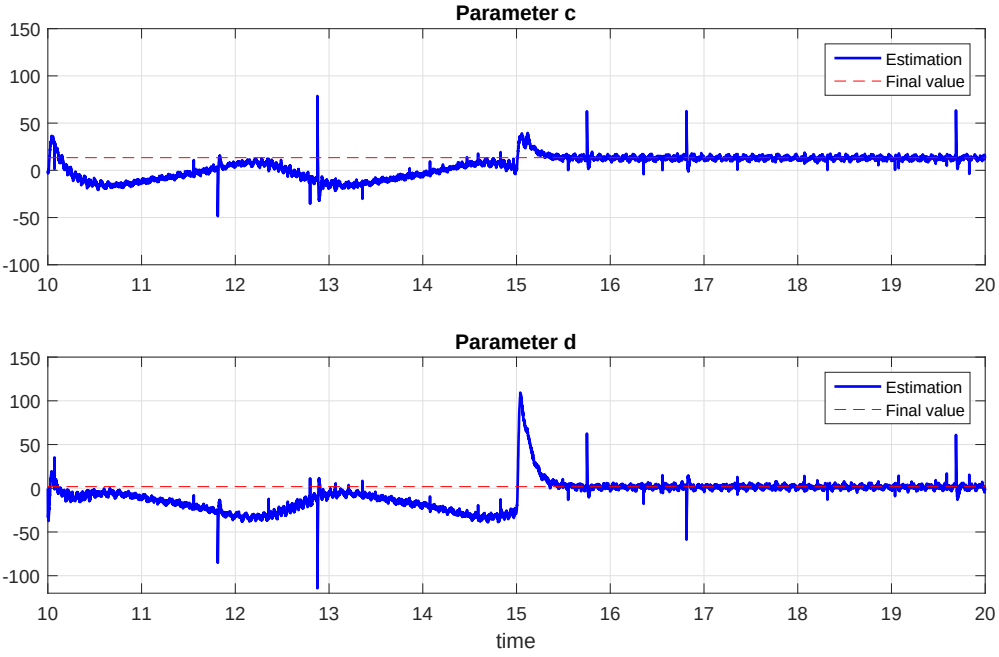

Figure 3.11: Estimates $\hat{c}$ and $\hat{d}$ obtained through the ARIM.

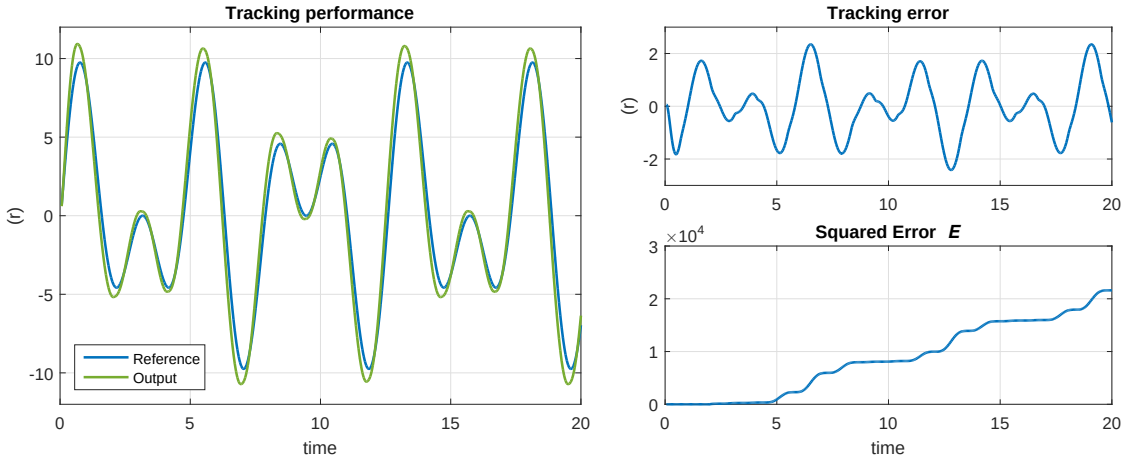

Figure 3.12: FSIM tracking performance.

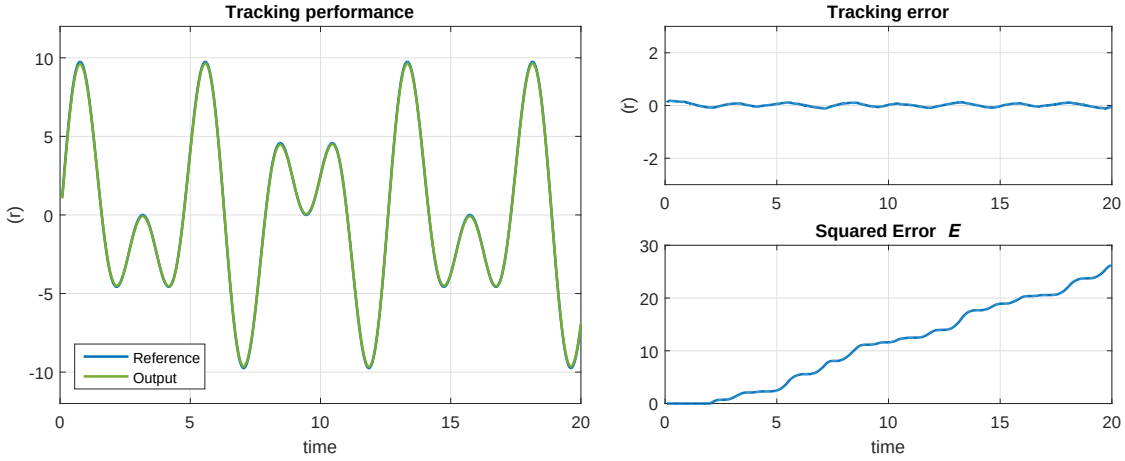

Figure 3.13: ARIM tracking performance.

On the other hand, the ARIM algorithm offers a higher accuracy because it uses a model including Coulomb friction c and constant disturbances d parameters, as shown in Fig. 3.13. However, it is clearly more complicated to use because the components of the regressor vector $\phi_A = [\phi_1(t) \;\; \phi_2(t)]^T$ require a special parameterization (B) that is obtained from the direct measurement of $q(t)$ and $u(t)$ signals. Furthermore, the excitation signal applied during the identification is more complex, as shown in Fig. 3.5 and Fig. 3.6. In this way, the choice of an adequate method essentially depends on the characteristics of the system under identification, the accuracy that is sought and the resources available for the implementation of the identification procedure.

3.4 Change of the parameters estimates due to magnetorheological damping

As an evidence of the versatility offered by the prototype used in this work, a change of the servomotor identified parameters is performed by means of the contribution of the magnetorheological damper $MD1$. As mentioned in chapter 2 the $MD1$ applies a magnetorheological damping directly to the motor shaft depending on the command voltage applied to the Wonder Box $W1$ (see Appendix A)

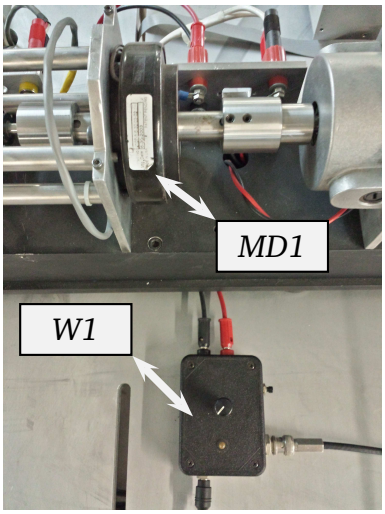

Figure 3.14: $MD1$ and $W1$ devices.

First, as it has been done so far, the inertia $J2$ is not added to the dynamic of the servomotor so that the clutch $C1$ remains disengaged. The outcomes for several voltage values are shown in Table 3.3 for the ARIM. For the second case, the inertia $J2$ is added to the dynamic of the servomotor by engaging the clutch $C2$. Table 3.4 shows the results obtained for several voltage values applied to the Wonder Box $W1$. Note that in both cases the ARIM produces reasonable estimates only when the $MD1$ is excited at low currents corresponding to low voltages applied to the Wonder Box $W1$.

W1	PD		Parameter identification				Performance
Voltage	K_p	K_d	$\hat{a}$	$\hat{b}$	$\hat{c}$	$\hat{d}$	E
0 V	20	0.46	0.458	170.9007	13.0808	1.8532	27.24
0.2 V	21	0.46	0.4646	170.7969	13.2555	1.8021	27.32
0.4 V	22	0.46	0.4923	169.0663	18.1405	1.3225	239.49
0.6 V	24	0.48	0.6003	156.2108	19.2509	1.2920	770.44
0.7 V*	26	0.50	1.2435	170.4798	36.5401	2.3373	8 737.00

Table 3.3: Results of ARIM with nominal inertia for several voltage values applied to the Wonder Box $W1$.

W1	PD		Parameter identification				Performance
Voltage	K_p	K_d	$\hat{a}$	$\hat{b}$	$\hat{c}$	$\hat{d}$	E
0 V	20.0	0.80	0.3020	82.3279	8.9221	0.9779	32.15
0.2 V	20.5	0.80	0.3067	82.2350	8.9384	0.9817	35.76
0.4 V	20.5	0.80	0.3149	82.1557	9.0356	0.9040	42.33
0.6 V	21.0	0.85	0.3573	82.1056	10.9133	0.8314	53.73
0.7 V*	22.0	0.85	0.3802	80.8019	18.9291	0.9497	404.73

Table 3.4: Results of ARIM with inertia $J2$ added, for several voltage values applied to the Wonder Box $W1$.

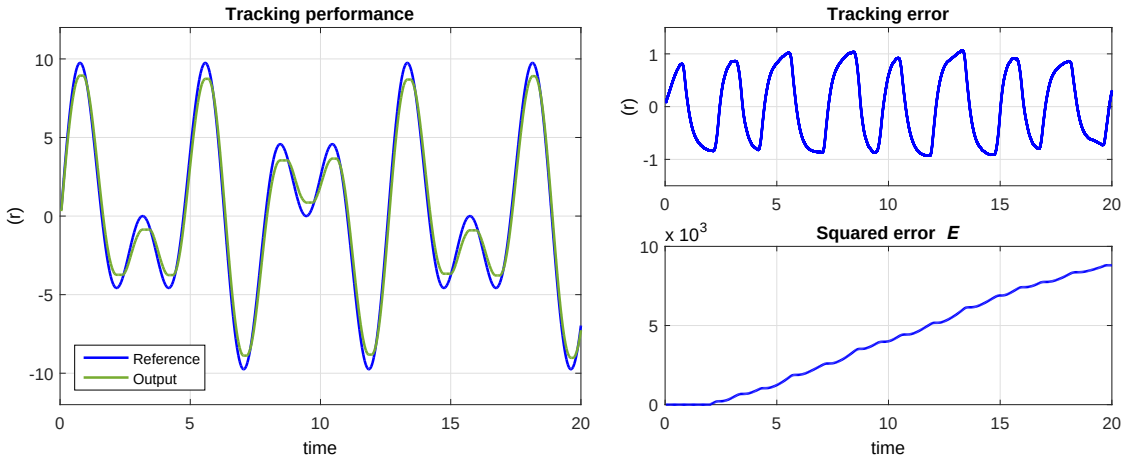

Figure 3.15: ARIM tracking performance with 0.7V excitation applied to $MD1$ and clutch $C1$ disengaged.

For the first and the second cases the squared error E remains below a value of 300 and 45, respectively, for excitation voltages up to 0.4 V, which is the range

where damping applied by $MD1$ is, roughly speaking, linear. Above this value the squared error E increases noticeably as shown in the Fig. 3.15 that depicts the tracking performance, the tracking error and the squared error. The above result indicates that the Bingham friction model (3.3) does not correctly describe the behavior of the $MD1$ for large values of the excitation voltage.

Additionally, note that for small excitation voltage, below 0.6 V, the value of the viscous friction coefficient in Table 3.3 is in the same range than the value of the derivative gain K_d used in the PD controller. This fact opens the possibility of injecting damping using the MD in a Proportional Integral Derivative (PID) controller instead of employing a classic derivative action.

CHAPTER 4

PARAMETER IDENTIFICATION OF THE PROTOTYPE CONSIDERING FLEXIBILITY

4.1 Prototype Section 1 plus Section 2 model

In this chapter the parameter identification of the whole prototype is studied, so that the clutch $C1$ is engaged and the clutch $C2$ is engaged for adding the contribution of the Section 2 and consequently obtaining a pair of equations coupled by means of the torque exerted by the spring S (see Fig. 4.1). The torque τ_s from the coupling works as the control signal applied to Section 2 and is described by the following equation

$$\tau_s = K_s \left(q_m(t) - q_s(t) \right) \tag{4.1}$$

where K_s, q_m and q_s represent the flexibility coefficient of the spring, the angular position of the servomotor shaft and the angular position of the inertia J_s, respectively (see Fig. 2.1).

The equation (4.2) describes the dynamics of the Section 1 of the prototype obtained adding the torque τ_s to the model (3.5) due to the spring coupling

$$J_m\ddot{q}_m(t) + f_m\dot{q}_m(t) + \mu_m \text{sign}\left(\dot{q}_m(t)\right) + \tau_s = Ku(t) + \tau_d \tag{4.2}$$

The second equation (4.3) of the model describes the dynamics of the Section 2 of the prototype considering the torque due to the spring S

$$\tau_s = J_s\ddot{q}_s + f\left(\dot{q}_s(t)\right) \tag{4.3}$$

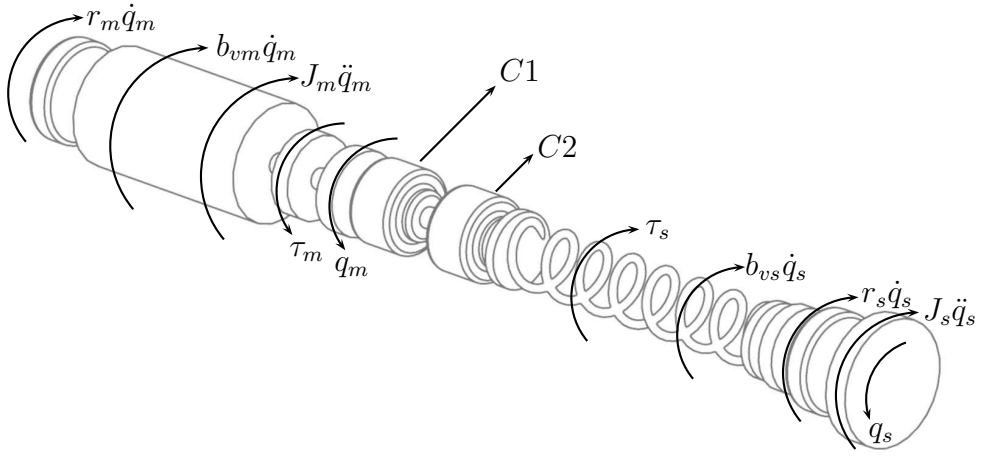

Figure 4.1: Mechanical system acting forces along the whole prototype.

Inertia J_s is the sum of the inertias $J3$ and $J4$. The Bingham model [27] is also used to describe the friction phenomena in the magnetorheological damper $MD2$. Thus the term $f\left(\dot{q}_s(t)\right)$ in (4.3) accounts for the mechanical and the magnetorheological friction

$$f\left(\dot{q}_s(t)\right) = f_s\dot{q}_s(t) + \mu_s \text{sign}\left(\dot{q}_s(t)\right) \tag{4.4}$$

The term f_s represents the viscous and the magnetorheological viscous friction coefficient, and the term μ_s represents the mechanical and the magnetorheological Coulomb friction coefficient.

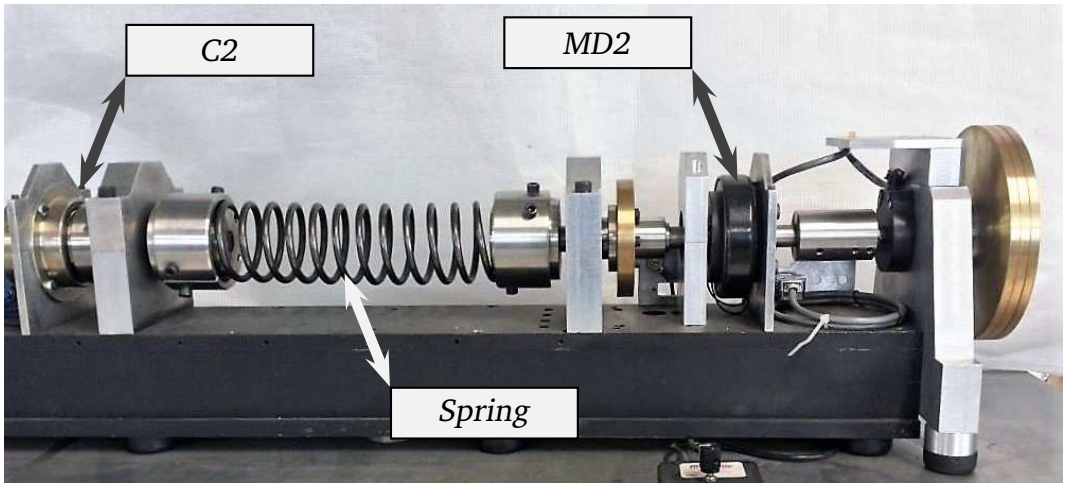

Figure 4.2: Section 2 of the prototype.

The sign$(\dot{q}_s(t))$ function is defined as

$$\text{sign}(\dot{q}_s(t)) = \begin{cases} 1, & \text{if} \quad \dot{q}_s(t) > 0 \\ 0, & \text{if} \quad \dot{q}_s(t) = 0 \\ -1, & \text{if} \quad \dot{q}_s(t) < 0 \end{cases} \tag{4.5}$$

Substituting equation (4.4) into equation (4.3) yields

$$J_s\ddot{q}_s(t) + f_s\dot{q}_s(t) + \mu_s\text{sign}\left(\dot{q}_s(t)\right) = \tau_s \tag{4.6}$$

Equations (4.2) and (4.6) shape the next model for the whole prototype

$$J_m\ddot{q}_m(t) + f_m\dot{q}_m(t) + \mu_m\text{sign}\left(\dot{q}_m(t)\right) + \tau_s = Ku(t) + \tau_d \tag{4.7a}$$

$$J_s\ddot{q}_s(t) + f_s\dot{q}_s(t) + \mu_s\text{sign}\left(\dot{q}_s(t)\right) = \tau_s \tag{4.7b}$$

which has the following alternative writing

$$\ddot{q}_m(t) = -a_m\dot{q}_m(t) + b_mu(t) - c_m\text{sign}\left(\dot{q}_m(t)\right) + d_m - g_m\left(q_m(t) - q_s(t)\right) \tag{4.8a}$$

$$\ddot{q}_s(t) = -a_s\dot{q}_s(t) + g_s\left(q_m(t) - q_s(t)\right) - c_s\text{sign}\left(\dot{q}_s(t)\right) \tag{4.8b}$$

with the next parameters definitions

$$\begin{aligned} a_m &= \frac{f_m}{J_m}; & b_m &= \frac{K}{J_m}; & c_m &= \frac{\mu_m}{J_m} \\ d_m &= \frac{\tau_d}{J_m}; & g_m &= \frac{K_s}{J_m}; & a_s &= \frac{f_s}{J_s} \\ g_s &= \frac{K_s}{J_s}; & c_s &= \frac{\mu}{J_s} \end{aligned} \tag{4.9}$$

4.2 Parameter identification

Based on the good performance shown by the ARIM in the experiments carried out in Section 3.3, a slight modification is performed to this method in order to identify the parameters of the whole prototype. It is necessary to stabilize the system as it was performed in Section **??** where the Section 1 of the prototype was stabilized by means of the PD controller (3.7). Moreover, the signal reference signal q_{rf1} (see Fig. 4.5) fulfills the Persistence of Excitation (PE) condition [45] and must be applied to the system under identification in the time interval $[0,\ t_0]$. The signal should enforce the prototype to rotate in only one direction thus making the Coulomb friction term sign$(\dot{q}_m)$ to have a constant value. If the stabilizing controller fulfills this condition, then it allows writing the model (4.8) as follows

$$\ddot{q}_m(t) = -a_m\dot{q}_m(t) + b_m u(t) + v_m - g_m\left(q_m(t) - q_s(t)\right) \tag{4.10a}$$

$$\ddot{q}_s(t) = -a_s\dot{q}_s(t) + g_s\left(q_m(t) - q_s(t)\right) + v_s \tag{4.10b}$$

where $v_m = -c_m\text{sign}\left(\dot{q}_m(t)\right) + d_m$ satisfies

$$v_m = \begin{cases} -c_m + d_m, & \dot{q}_m(t) > 0 \\ c_m + d_m, & \dot{q}_m(t) < 0 \end{cases} \tag{4.11}$$

and $v_s = -c_s \text{sign}\left(\dot{q}_s(t)\right)$ satisfies

$$v_s = \begin{cases} -c_s, & \dot{q}_s(t) > 0 \\ c_s, & \dot{q}_s(t) < 0 \end{cases} \tag{4.12}$$

A regression model for the equations set (4.10) obtained using the operational calculus corresponds to

$$z_m(t) = \theta_m^T \phi_m(t) \tag{4.13}$$

$$\phi_m(k) = [\phi_{11}(k) \;\; \phi_{12}(k) \;\; \phi_{13}(k)]^T \qquad \theta_m = [a_m \;\; b_m \;\; g_m]^T$$

$$z_s(t) = \theta_s^T \phi_s(t) \tag{4.14}$$

$$\phi_s(k) = [\phi_{21}(k) \;\; \phi_{22}(k)]^T \qquad \theta_s = [a_s \;\; g_s]^T$$

where (see Appendix C)

$$z_1(t) = a_m \phi_{11}(t) + b_m \phi_{12}(t) + g_m \phi_{13}(t) \tag{4.15}$$

$$\begin{aligned} z_1(t) &= t^3 q_m - 9 \int t^2 q_m + 18 \int^{(2)} t q_m - 6 \int^{(3)} q_m \\ \phi_{11}(t) &= - \int t^3 q_m + 6 \int^{(2)} t^2 q_m - 6 \int^{(3)} t q_m \\ \phi_{12}(t) &= \int^{(2)} t^3 u - 3 \int^{(3)} t^2 u \\ \phi_{13}(t) &= - \int^{(2)} t^3 q_{ef} + 3 \int^{(3)} t^2 q_{ef} \end{aligned}$$

$$z_2(t) = a_s \phi_{21}(t) + g_s \phi_{22}(t) \tag{4.16}$$

$$\begin{aligned} z_2(t) &= t^3 q_s - 9 \int t^2 q_s + 18 \int^{(2)} t q_s - 6 \int^{(3)} q_s \\ \phi_{21}(t) &= - \int t^3 q_s + 6 \int^{(2)} t^2 q_s - 6 \int^{(3)} t q_s \\ \phi_{22}(t) &= \int^{(2)} t^3 q_{ef} - 3 \int^{(3)} t^2 q_{ef} \end{aligned}$$

The operator $\int^{(n)} \rho(t)$ represents the iterated integral $\int_0^t \int_0^{\tau_1} \dots \int_0^{\tau_{n-1}} \rho(\tau_n) d\tau_n \dots d\tau_2 \tau_1$. The regression models (4.13) and (4.14) are valid for the time instants $t = T, 2T, ..., (K-1)T, KT, ...$ where T is the sampling period, i.e.

$$z_1(KT) = \theta_m^T \phi_m(KT) \tag{4.17a}$$

$$z_2(KT) = \theta_s^T \phi_s(KT) \tag{4.17b}$$

or simply

$$z_1(K) = \theta_m^T \phi_m(K) \tag{4.18a}$$

$$z_2(K) = \theta_s^T \phi_s(K) \tag{4.18b}$$

On the other hand, the vector Ω_i satisfies the Persistence of Excitation condition [45] if

$$\lim_{k\to\infty} \Omega_i = \lim_{k\to\infty} \lambda_{min} \left[\sum_{j=1}^{k} A_i(j) \right] = \infty \tag{4.19}$$

being

$$A_i(j) = \phi_i(j) \phi_i^T(j) \tag{4.20}$$

where $\lambda_{min}[\cdot]$ stands for smallest eigenvalue and the subscript $i = m, s$ corresponds to the regressors (4.18a) and (4.18b), respectively. Furthermore, the next standard Recursive Least Squares algorithm (see [44] and [45]) is performed for each one of the regression models (4.18)

$$\begin{aligned}
\hat{\theta}_i(k) &= \hat{\theta}_i(k-1) + L_i(k)\epsilon(k) \\
L_i(k) &= \frac{P_i(k-1)\phi_i(k)}{1 + \phi_i^T(k) P_i(k-1) \phi(k)} \\
P_i(k) &= P_i(k-1) + \frac{P_i(k-1)\phi_i(k)\phi_i^T(k)P_i(k-1)}{1 + \phi_i^T(k) P_i(k-1) \phi_i(k)} \\
\epsilon_i(k) &= z_i(k) - \phi_i^T(k) \hat{\theta}_i(k-1)
\end{aligned} \tag{4.21}$$

where the subscript $i = m, s$ also corresponds to the Recursive Least Square algorithm applied to the regressors (4.18a) and (4.18b) respectively. Moreover, the terms $\hat{\theta}_i$ are the estimates of θ_i, P_i are the covariance gain matrices and ϵ_i are the estimation errors.

In the second step of the identification procedure the estimates $\hat{c}_m$, $\hat{d}_m$ and $\hat{c}_s$ are computed using the reference signal q_{rf2} (see Fig. 4.6) during the time interval $[t_0,\, t_1]$. The following set of conditions hold at the end oh the time interval $t \in [t_0,\, t_0 + \delta]$ and $t \in [t_0 + \delta,\, t_1]$ respectively

$$\left.\begin{aligned} \dot{q}_m(t), \dot{q}_s(t) &= m \\ \text{sign}\left(\dot{q}_m(t)\right), \text{sign}\left(\dot{q}_s(t)\right) &= 1 \\ \ddot{q}_m(t), \ddot{q}_s(t) &= 0 \\ u(t) &= u^*_+ \\ \left(q_m(t) - q_s(t)\right) &= q_{ef_+} \end{aligned}\right\} \quad t \in [t_0,\, t_0 + \delta]$$

$$\left.\begin{aligned} \dot{q}_m(t), \dot{q}_s(t) &= -m \\ \text{sign}\left(\dot{q}_m(t)\right), \text{sign}\left(\dot{q}_s(t)\right) &= -1 \\ \ddot{q}_m(t), \ddot{q}_d(t) &= 0 \\ u(t) &= u^*_- \\ \left(q_m(t) - q_s(t)\right) &= q_{ef_-} \end{aligned}\right\} \quad t \in [t_0 + \delta,\, t_1]$$

Substituting each one of above cases in (4.8) produces the sets of equations

$$c_m - d_m = -a_m m + b_m u^*_+ - g_m q_{ef_+} \tag{4.22a}$$

$$c_s = -a_s m + g_s q_{ef_+} \tag{4.22b}$$

and

$$-c_m - d_m = a_m m + b_m u^*_- - g_m q_{ef_-} \tag{4.23a}$$

$$-c_s = a_s m + g_s q_{ef_-} \tag{4.23b}$$

Solving (4.22) and (4.23) for $\hat{c}_m$, $\hat{d}_m$ and $\hat{c}_s$ yields

$$\hat{c}_m = -\hat{a}_m m + \hat{b}_m u_+^* - \hat{g}_m q_{ef_+} + \hat{d}_m \tag{4.24a}$$

$$\hat{d}_m = -\frac{1}{2}\left[\hat{b}_m\left(u_+^* + u_-^*\right) + \hat{g}_m\left(q_{ef_+} + q_{ef_-}\right)\right] \tag{4.24b}$$

$$\hat{c}_s = -\hat{a}_s m - \hat{g}_s q_{ef_-} \tag{4.24c}$$

The parameters c_s and c_m are obtained directly from (4.22). It is also possible to obtain c_s from (4.23) since both sets of equations describe the same model at different time instants.

4.3 Stabilization of the system

It is necessary to stabilize the prototype without previous knowledge of its parameters in order to apply the identification method described in Section 4.2. To this end, consider the prototype model (4.8) and define the state variables

$$x^T(t) = [q_m(t) \quad \dot{q}_m(t) \quad q_s(t) \quad \dot{q}_s(t)] \tag{4.25}$$

The above definitions allow writing the next state-space model

$$\dot{x}(t) = Ax(t) + bu(t) + s \tag{4.26a}$$

$$y(t) = cx(t) \tag{4.26b}$$

where

$$A = \begin{bmatrix} 0 & 1 & 0 & 0 \\ -g_m & -a_m & g_m & 0 \\ 0 & 0 & 0 & 1 \\ g_s & 0 & -g_s & -a_s \end{bmatrix}; \qquad b = \begin{bmatrix} 0 \\ b_m \\ 0 \\ 0 \end{bmatrix}; \qquad c = \begin{bmatrix} 0 \\ 0 \\ 1 \\ 0 \end{bmatrix}^T \tag{4.27}$$

and

$$s = \begin{bmatrix} 0 \\ -c_m \text{sign}(\dot{q}_m(t)) + d_m \\ 0 \\ -c_s \text{sign}(\dot{q}_s(t)) \end{bmatrix} \tag{4.28}$$

The vector s (4.28) is bounded and contains the non-linear terms in (4.8) and the bounded disturbances acting in the linear system (4.27). The characteristic polynomial of the matrix A is

$$\begin{aligned} \det(sI - A) &= s^4 + (a_m + a_s)^3 + (g_m + g_s + a_m a_s)s^2 + (a_m g_s + a_s g_m)s \\ &= s\left[s^3 + (a_m + a_s)^2 + (g_m + g_s + a_m a_s)s + a_m g_s + a_s g_m\right] \end{aligned} \tag{4.29}$$

The above polynomial shows that the open-loop system is not asymptotically stable, there exists an eigenvalue placed in $s = 0$ and the system is marginally stable [46]. The controllability is the ability to transfer a system from any initial state $x(0) = x_0$ to any desired final state $x(t_f) = x_f$ within a finite time interval, i.e. for $t_f < \infty$ [50], then it is necessary to make sure that the system is controllable and consequently is able to be stabilized [51]. A linear system is controllable if and only if the associated controllability matrix $\mathcal{C} = [B \;\; AB \;\; A^2B \;\; A^3B]$ has full-rank. Thereby, the controllability matrix associated to the model (4.27) corresponds to

$$\mathcal{C} = \begin{bmatrix} 0 & b_m & -b_m a_m & -b_m(g_m - {a_m}^2) \\ b_m & -b_m a_m & -b_m(g_m - {a_m}^2) & b_m a_m(2g_m - {a_m}^2)) \\ 0 & 0 & 0 & b_m g_s \\ 0 & 0 & b_m g_s & -b_m g_s(a_m + a_s) \end{bmatrix} \tag{4.30}$$

and its determinant is

$$\det(\mathcal{C}) = {b_m}^4 {g_s}^2 \tag{4.31}$$

The value of g_s depends on the spring coefficient K_s (see equations (4.9)) and the input gain b_m. The fact that they are positives constants ensures that $\mathcal{C}$ is a full-rank matrix

and the system is controllable [46], which means that its stabilization is possible by using a state-feedback control law. Stabilization of (4.27) is achieved by means of the following parallel PD controller

$$u(t) = k_{pm}\left[q_{rf}(t) - q_m(t)\right] - k_{dm}\dot{q}_m(t) + k_{ps}\left[q_{rf}(t) - q_s(t)\right] - k_{ds}\dot{q}_s(t) \tag{4.32}$$

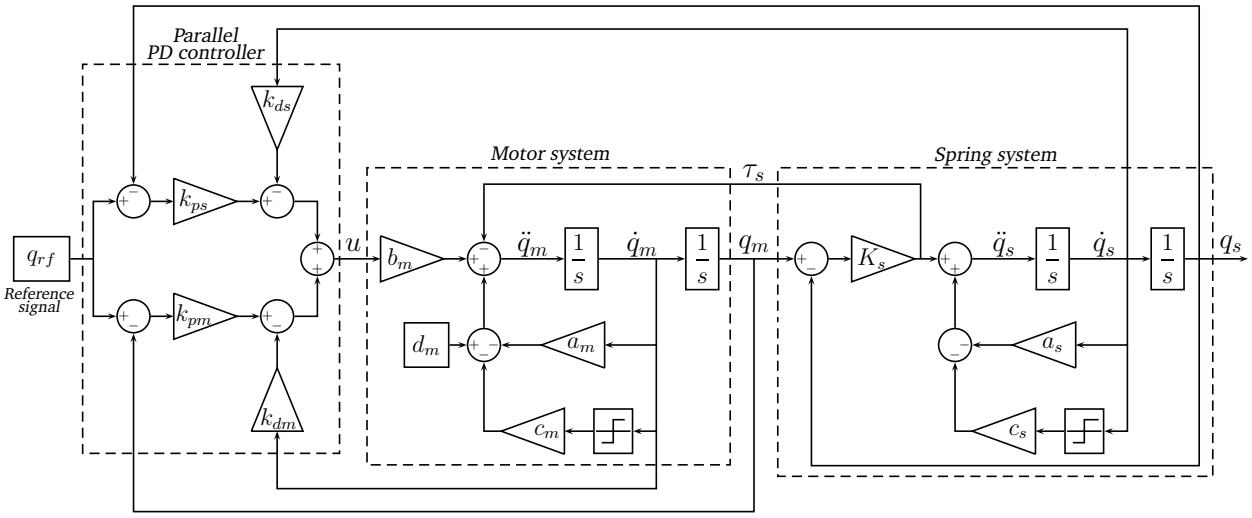

Figure 4.3: Parallel PD controller (4.32) used for stabilizing the model (4.8).

being k_{pm}, k_{dm}, k_{ps} and k_{ds} positive constants. If the reference signal $q_{rf}(t)$ is equal to zero then the control law (4.32) becomes

$$u(t) = -k_{pm}q_m(t) - k_{dm}\dot{q}_m(t) - k_{ps}q_s(t) - k_{ds}\dot{q}_s(t) \tag{4.33}$$

which corresponds to the state-feedback control law [52]

$$u(t) = -K^T x(t) \tag{4.34}$$

with

$$K^T = [k_{pm} \quad k_{dm} \quad k_{ps} \quad k_{ds}] \tag{4.35}$$

The results obtained throughout the stability analysis detailed in Appendix D show that it is possible to stabilize system (4.8) using a state-feedback gain high enough.

Therefore, by gradually increasing the feedback gains it is possible to stabilize the system even if its parameters are unknown. So, the controller (4.32) applied to the system (4.8) is tuned through a trial and error process. First the proportional gains k_{pm} and k_{ps} are increased until the system response presents oscillations and then the derivatives gains k_{dm} and k_{ds} are increased to reduce the overshoot. Fig. 4.4 shows the outcome of the system stabilized through the parallel PD controller (4.32) tuned with the gains (4.36) and using a filtered square wave as a reference.

$$\begin{aligned} K_{pm} &= 15 & K_{ps} &= 21 \\ K_{dm} &= 13.5 & K_{ds} &= 4 \end{aligned} \tag{4.36}$$

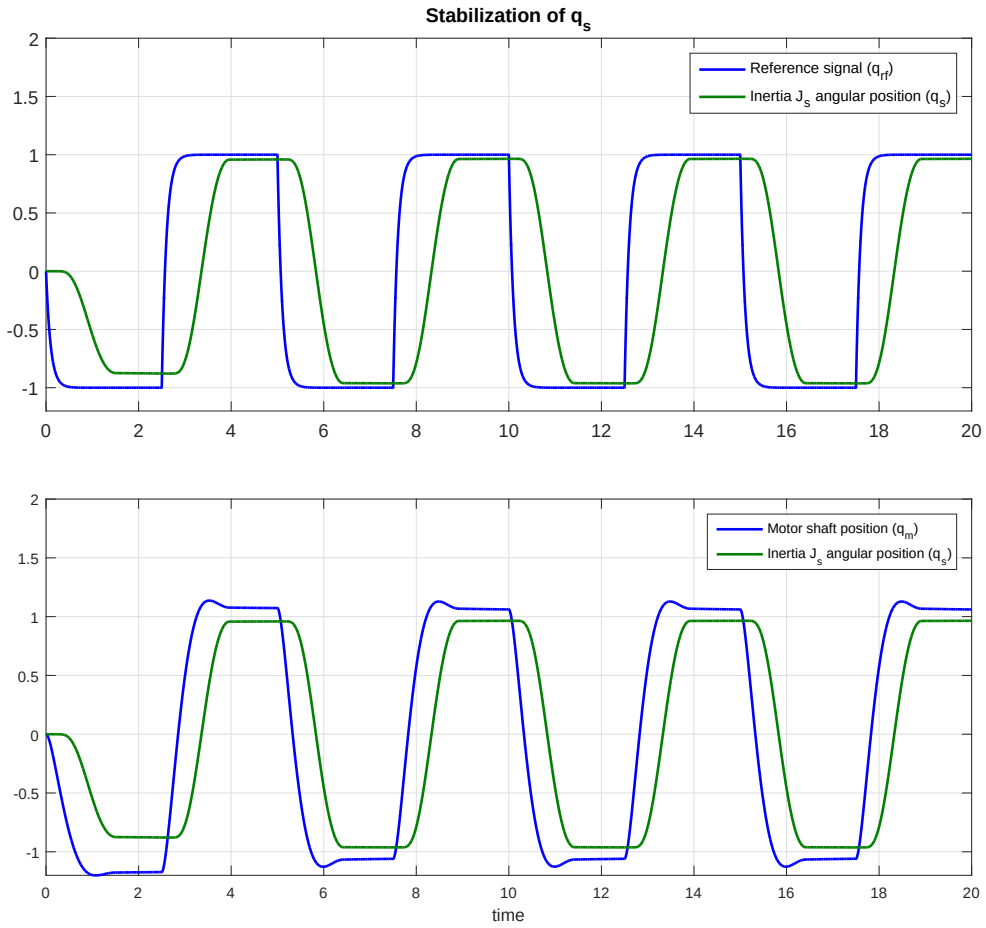

Figure 4.4: Simulation response of the prototype stabilized through the controller (4.32).

4.4 Simulation setting

The modified ARIM employs the excitation signal

$$\begin{aligned} q_{rf1} =& 18t + 0.25\sin(1.7\pi t) + 4\sin(0.8\pi t) \\ &+ 2\sin(1.2\pi t) + 2\sin(2\pi t) + 0.56\mathcal{R} \end{aligned} \tag{4.37}$$

that is shown in Fig. 4.5 with $t_0 = 10\,s$, i.e., during the time interval $[0\,s,\ 10\,s]$ where $\mathcal{R}$ is a Matlab Band-Limited White Noise block with a power noise of 0.56 and a sample time of $0.1\,s$. The inertia values for the calculation of g_m and g_s are $J_m = 0.5$ and $J_s = 0.2$. The solver ODE1-Euler with a fixed step size of $0.001\,s$ is used for implementing the regressors (4.18a) and (4.18b). The signal q_{rf2} depicted in Fig. 4.6 is applied to the system with $t_1 = 20\,s$, i.e., within the time interval $[10\,s,\ 20\,s]$. The Least Square algorithm (4.21) uses the covariance gain matrices $P_i(0) = \text{diag}[10\,000,\ 10\,000]$ and the initial estimated values $\theta_i(0) = [0,\ 0]^T$ for $i = m, s$.

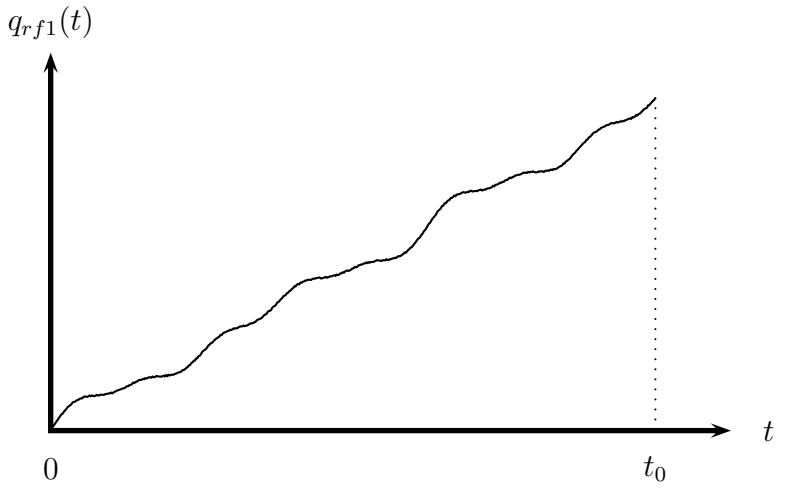

Figure 4.5: Reference signal q_{rf1} used for $\hat{a}_m$, $\hat{b}_m$, $\hat{g}_m$, $\hat{a}_s$ and $\hat{g}_s$ estimation.

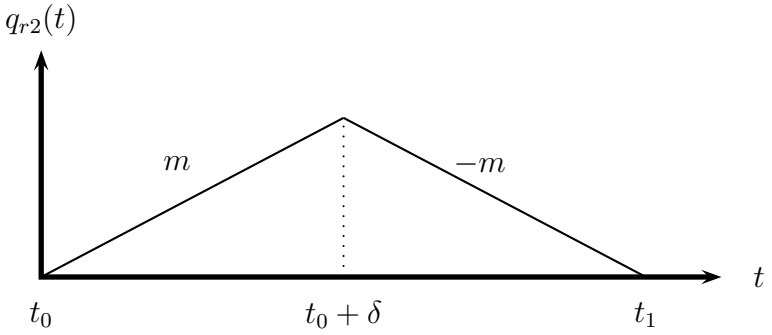

Figure 4.6: Reference signal q_{rf2} used for $\hat{c}_m$, $\hat{d}_m$ and $\hat{c}_s$ estimation.

4.5 Results

The real and the estimated parameters for simulation are shown in Table 4.1, Fig. 4.7 and Fig. 4.8. Furthermore, Fig. 4.9 and 4.10 evidence that the values of Ω_m and Ω_s in (4.19) would tend to infinity when $k \to \infty$, thus the regressors (4.18a) and (4.18b) are likely to satisfy the Persistence of Excitation condition.

Parameter identification			
Parameter	Real values	Estimated values	% error
$\hat{a}_m$	2	1.9704	1.4799
$\hat{b}_m$	50	49.9562	0.0876
$\hat{c}_m$	10	10.2192	2.1920
$\hat{d}_m$	1.7	1.7239	1.4071
$\hat{g}_m$	26	26.0944	0.3633
$\hat{a}_s$	3	2.9866	0.4469
$\hat{g}_s$	65	64.9770	0.0354
$\hat{c}_s$	6	5.9746	0.4230

Table 4.1: Parameters estimates obtained when the Section 1 and the Section 2 of the prototype work together.

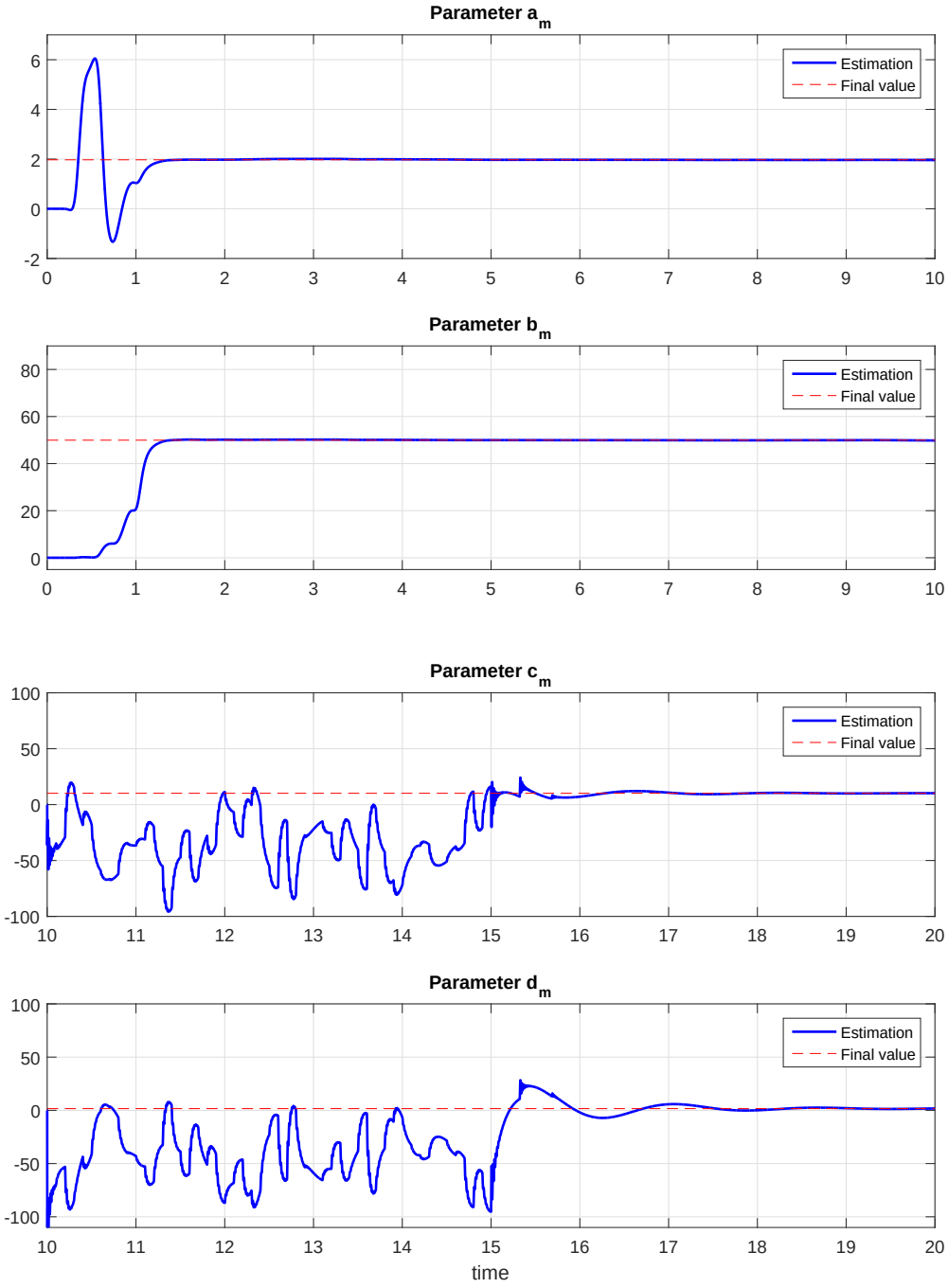

Figure 4.7: Estimates $\hat{a}_m$, $\hat{b}_m$, $\hat{c}_m$ and $\hat{d}_m$ obtained through the modified ARIM.

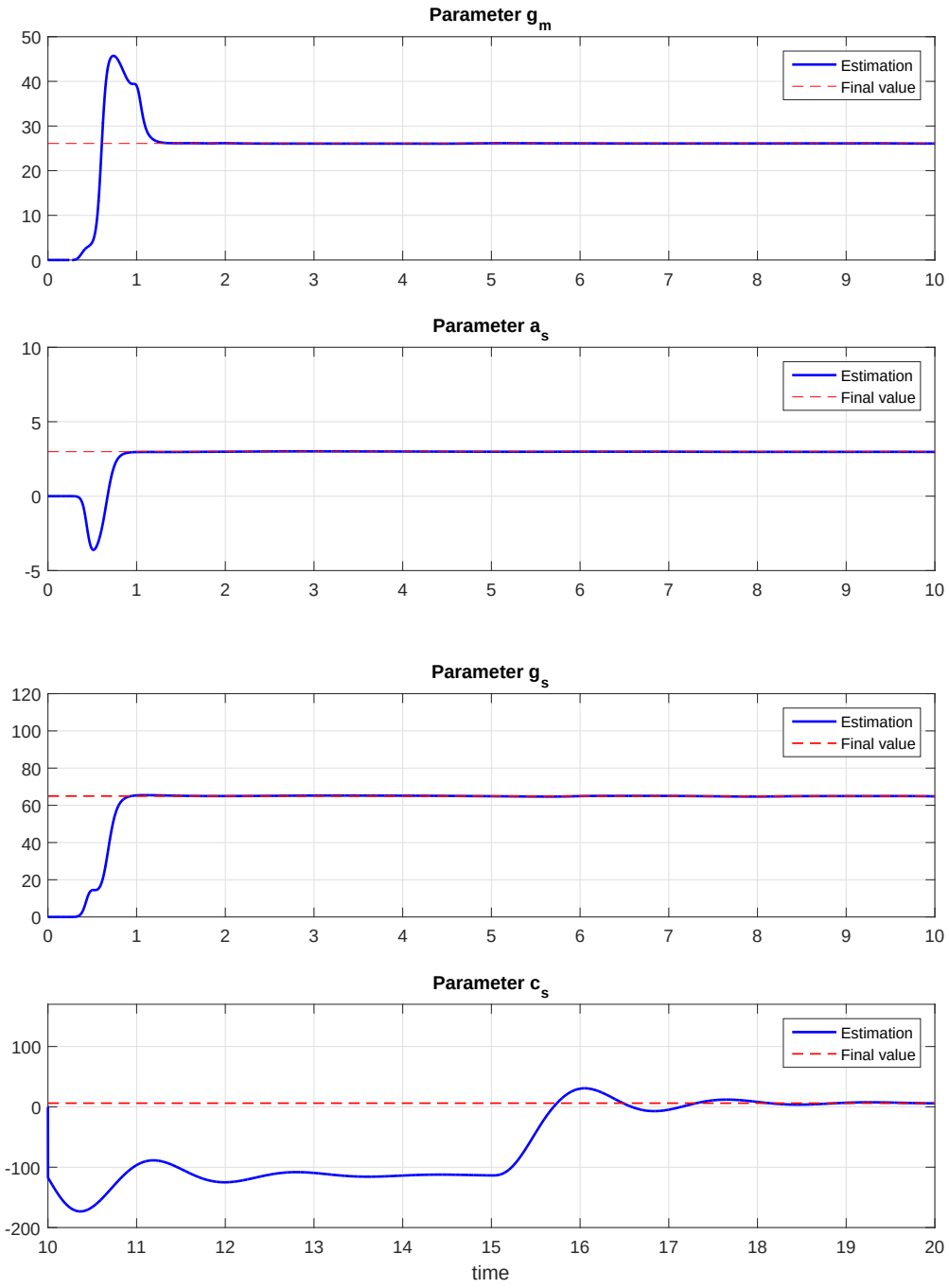

Figure 4.8: Estimates $\hat{g}_m$, $\hat{a}_s$, $\hat{g}_s$ and $\hat{c}_s$ obtained through the modified ARIM.

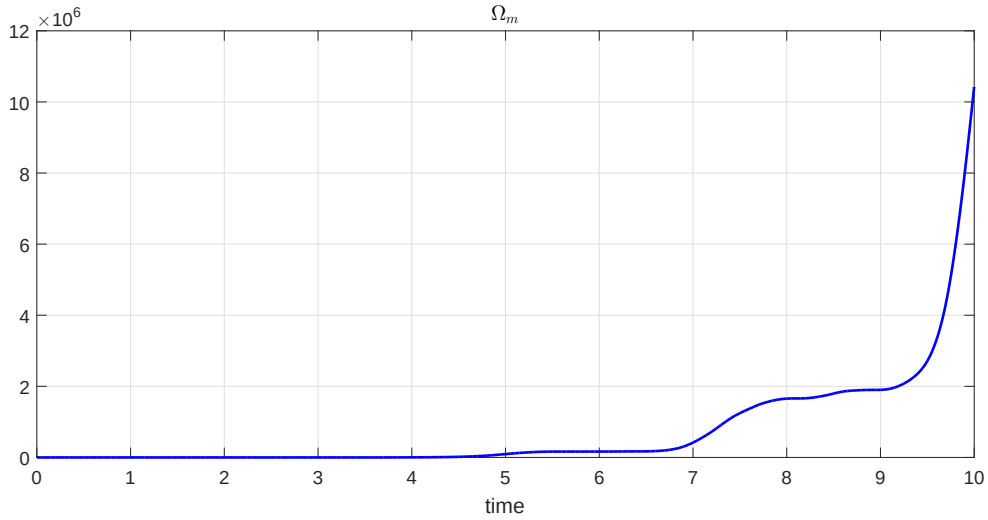

Figure 4.9: Performance of the Persistence of Excitation condition (4.19) for the regressor (4.18a).

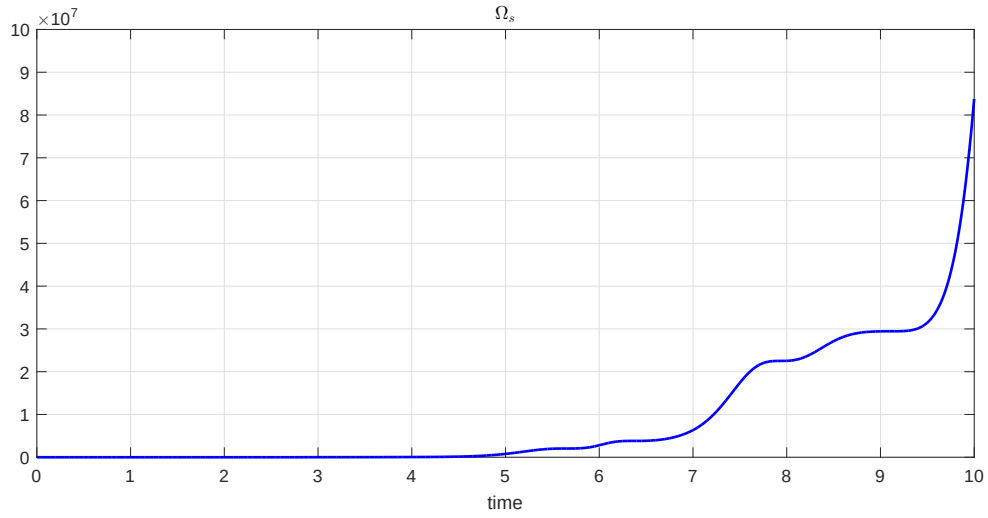

Figure 4.10: Performance of the Persistence of Excitation condition (4.19) for the regressor (4.18b).

4.5.1 Remarks

The model (4.8) is obtained when the Section 1 and the Section 2 of the prototype are engaged, adding the spring flexibility to the dynamics of the system. The stabilization of

the system is achieved by means of the parallel PD controller (4.32), which is tuned by means of a trial and error process. Once the system is stabilized, it is possible to apply the identification method proposed in Section 4.2. Moreover, Table 4.1 shows that the parametric errors stay below 2.2% for each one of the parameters, so that the modified ARIM algorithm proposed in Section 4.2 seems to be a suitable identification method to be applied to the laboratory prototype.

CHAPTER 5

CONCLUSIONS

Along the experiments carried out in Chapter 3 it is clear that, in the case when the servomechanism is driving an inertia load and is coupled to a magnetorheological damper the four-parameter model, which includes Bingham friction model, viscous and Coulomb friction, and constant disturbances, is a meaningful more precise model for parameter identification than the two-parameter model that only includes the viscous friction. This statement is based on the values of the squared tracking error E produced by the parameters obtained by means of both models, when they are used to design a control law aimed to a trajectory tracking control problem. The experimental results evidence that the Bingham model describes reasonably well the magnetorheological damper friction only at low excitation voltages, up to 0.6 V. More complicated models that include the hysteretic nature of the magnetorheological damper friction seem necessary for describing the behavior of the MD at higher excitation values. These could be the Bouc-Wen, the modified Bouc-Wen or the Dahl models. However, the results presented here open the possibility of using a magnetorheological damper at low excitation voltages for injecting damping to a servomotor instead of using the traditional Derivative action in a Proportional Integral Derivative (PID) controller.

The modification proposed for the ARIM in order to identify the parameters of the whole prototype considering the flexibility introduced by spring and without exciting the MD, seems to be an adequate identification method since the simulation results show that the algorithm delivers estimates parameters within a margin error of 2.2%. This fact gives a good panorama about how the modified ARIM works, so that the next natural step would be to prove this algorithm in real-time experiments. In order to perform the parameter identification for the whole prototype, it is stabilized without knowledge on its parameters using a Parallel Proportional Derivative (PPD) controller. Its tuning is accomplished by gradually increasing the control gains, and this tuning method is supported by a stability analysis performed using the Lyapunov second method.

Finally, this work provides a first glance of the versatility of the research areas that can be addressed with the laboratory prototype employed in this work.

According to the comments in the preceding paragraphs, future work includes

- To identify in real-time the parameters of a hysteretic model of a magnetorheological damper.
- To identify in real-time the parameters of the whole prototype including flexibility torques.
- To develop a control law applied to a servomotor, endowed with a magnetorheological damper, taking advantage of the capability of the latter to change its friction levels by means of a control voltage.

APPENDICES

APPENDIX A

MAGNETORHEOLOGICAL DAMPER

Torque-current-command voltage correspondence for the magnetorheological dampers $MD1$ and $MD2$ and the WonderBox $W1$ and $W2$

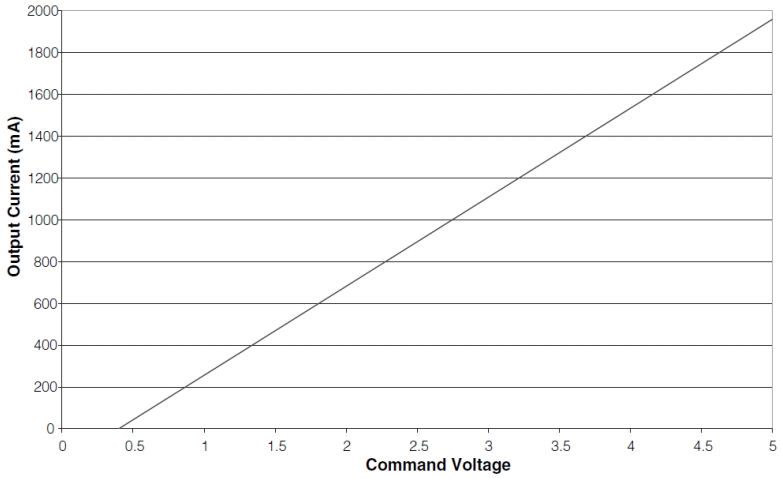

Figure 1: WonderBox current response.

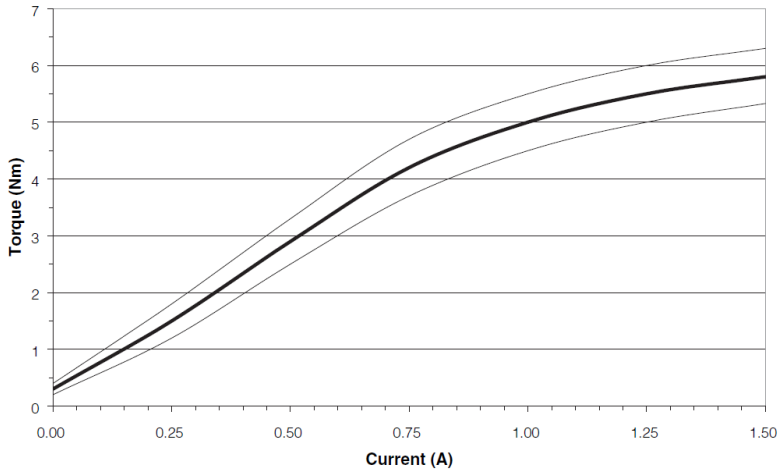

Figure 2: Magnetorheological damper torque as a function of the current.

APPENDIX B

SYSTEM PARAMETERIZATION

The Laplace transform of (3.20) is

$$s^2 Q_m(s) - s q_m(0) - \dot{q}_m(0) = -a\left[sQ_m(s) - q(0)\right] + bU(s) + \frac{\nu}{s} \tag{1}$$

where $Q_m(s)$ and $U(s)$ are the Laplace transforms of $q_m(t)$ and $u(t)$ respectively. Multiplying equation (1) by s leads to

$$s^3 Q_m(s) - s^2 q_m(0) - s\dot{q}_m(0) = -a\left[s^2 Q_m(s) - sq(0)\right] + bsU(s) + \nu \tag{2}$$

Deriving (2) three times, the initial conditions and term ν are canceled out

$$\frac{d^3}{ds^3}\left[s^3 Q_m(s)\right] = -a\frac{d^3}{ds^3}\left[s^2 Q_m(s)\right] + b\frac{d^3}{ds^3}\left[sU(s)\right] \tag{3}$$

where:

$$\frac{d^3}{ds^3}\left[s^3 Q_m(s)\right] = s^3\frac{d^3}{ds^3}Q_m(s) + 9s^2\frac{d^2}{ds^2}Q_m(s) + 18s\frac{d}{ds}Q_m(s) + 6Q_m(s) \tag{4a}$$

$$\frac{d^3}{ds^3}\left[s^2 Q_m(s)\right] = s^2\frac{d^3}{ds^3}Q_m(s) + 6s\frac{d^2}{ds^2}Q_m(s) + 6\frac{d}{ds}Q_m(s) \tag{4b}$$

$$\frac{d^3}{ds^3}\left[sU(s)\right] = s\frac{d^3}{ds^3}U(s) + 3\frac{d^2}{ds^2}U(s) \tag{4c}$$

Replacing the set of equations (4) in (3) yields

$$\begin{aligned} s^3\frac{d^3}{ds^3}Q_m(s) + 9s^2\frac{d^2}{ds^2}Q_m(s) + 18s\frac{d}{ds}Q_m(s) + 6Q_m(s) = \\ -a\left[s^2\frac{d^3}{ds^3}Q_m(s) + 6s\frac{d^2}{ds^2}Q_m(s) + 6\frac{d}{ds}Q_m(s)\right] \\ +b\left[s\frac{d^3}{ds^3}U(s) + 3\frac{d^2}{ds^2}U(s)\right] \end{aligned} \tag{5}$$

Multiplying (5) by s^{-3} produces

$$\begin{aligned}\frac{d^3}{ds^3}Q_m(s) + 9s^{-1}\frac{d^2}{ds^2}Q_m(s) + 18s^{-2}\frac{d}{ds}Q_m(s) + 6s^{-3}Q_m(s) = \\ -a\left[s^{-1}\frac{d^3}{ds^3}Q_m(s) + 6s^{-2}\frac{d^2}{ds^2}Q_m(s) + 6s^{-3}\frac{d}{ds}Q_m(s)\right] \\ +b\left[s^{-2}\frac{d^3}{ds^3}U(s) + 3s^{-3}\frac{d^2}{ds^2}U(s)\right]\end{aligned} \tag{6}$$

Applying the inverse Laplace transform to equation (6) leads to obtain the next parameterization (see [43])

$$z(t) = a\phi_1(t) + b\phi_2(t)$$

$$\begin{aligned}z(t) &= t^3 q_m - 9\int t^2 q_m + 18\int^{(2)} t q_m - 6\int^{(3)} q_m \\ \phi_1(t) &= -\int t^3 q_m + 6\int^{(2)} t^2 q_m - 6\int^{(3)} t q_m \\ \phi_2(t) &= \int^{(2)} t^3 u - 3\int^{(3)} t^2 u\end{aligned}$$

APPENDIX C

PARAMETERIZATION OF THE PROTOTYPE MODEL (4.8)

Through the application of the reference signal q_{rf1}, the model (4.8) corresponds to

$$\ddot{q}_m(t) = -a_m\dot{q}_m(t) + b_m u(t) + v_m - g_m\left(q_m(t) - q_s(t)\right) \tag{7a}$$

$$\ddot{q}_s(t) = -a_s\dot{q}_s(t) + g_s\left(q_m(t) - q_s(t)\right) + v_s \tag{7b}$$

where $v_m = -c_m\text{sign}\left(\dot{q}_m(t)\right) + d_m$ and $v_s = -c_s\text{sign}\left(\dot{q}_s(t)\right)$ satisfy

$$v_m = \begin{cases} -c_m + d_m, & \dot{q}_m(t) > 0 \\ c_m + d_m, & \dot{q}_m(t) < 0 \end{cases} \tag{8}$$

$$v_s = \begin{cases} -c_s, & \dot{q}_s(t) > 0 \\ c_s, & \dot{q}_s(t) < 0 \end{cases} \tag{9}$$

being $q_{ef}(t) = q_m(t) - q_s(t)$, the Laplace transform of the set of equations (7) yields

$$\begin{aligned} s^2Q_m(s) - sq_m(0) - \dot{q}_m(0) = &- a_m\left[sQ_m(s) - q_m(0)\right] + b_mU(s) \\ &+ \frac{v_m}{s} - g_mQ_{ef}(s) \end{aligned} \tag{10a}$$

$$s^2Q_s(s) - sq_s(0) - \dot{q}_s(0) = - a_s\left[sQ_s(s) - q_s(0)\right] + g_sQ_{ef}(s) + \frac{v_s}{s} \tag{10b}$$

where $Q_{ef}(s)$, and $U(s)$ are the Laplace transforms of $q_{ef}(t)$ and $u(t)$ respectively. Multiplying the set of equations (10) by s leads to

$$\begin{aligned} s^3Q_m(s) - s^2q_m(0) - s\dot{q}_m(0) = &- a_m\left[s^2Q_m(s) - sq_m(0)\right] + b_msU(s) \\ &+ v_m - g_msQ_{ef}(s) \end{aligned} \tag{11a}$$

$$s^3Q_s(s) - s^2q_s(0) - s\dot{q}_s(0) = - a_s\left[s^2Q_s(s) - sq_s(0)\right] + g_ssQ_{ef}(s) + v_s \tag{11b}$$

The initial conditions and the terms v_m and v_s are canceled out as follows

$$\frac{d^3}{ds^3}\left[s^3 Q_m(s)\right] = -a_m \frac{d^3}{ds^3}\left[s^2 Q_m(s)\right] + b_m \frac{d^3}{ds^3}\left[sU(s)\right] - g_m \frac{d^3}{ds^3}\left[sQ_{ef}(s)\right] \tag{12a}$$

$$\frac{d^3}{ds^3}\left[s^3 Q_s(s)\right] = -a_s \frac{d^3}{ds^3}\left[s^2 Q_s(s)\right] + g_s \frac{d^3}{ds^3}\left[sQ_{ef}(s)\right] \tag{12b}$$

Each term of (12a) is equal to

$$\frac{d^3}{ds^3}\left[s^3 Q_m(s)\right] = s^3 \frac{d^3}{ds^3} Q_m(s) + 9s^2 \frac{d^2}{ds^2} Q_m(s) + 18s \frac{d}{ds} Q_m(s) + 6Q_m(s) \tag{13a}$$

$$\frac{d^3}{ds^3}\left[s^2 Q_m(s)\right] = s^2 \frac{d^3}{ds^3} Q_m(s) + 6s \frac{d^2}{ds^2} Q_m(s) + 6 \frac{d}{ds} Q_m(s) \tag{13b}$$

$$\frac{d^3}{ds^3}\left[sU(s)\right] = s \frac{d^3}{ds^3} U(s) + 3 \frac{d^2}{ds^2} U(s) \tag{13c}$$

$$\frac{d^3}{ds^3}\left[sQ_{ef}(s)\right] = s \frac{d^3}{ds^3} Q_{ef}(s) + 3 \frac{d^2}{ds^2} Q_{ef}(s) \tag{13d}$$

and each term of (12b) is equal to

$$\frac{d^3}{ds^3}\left[s^3 Q_s(s)\right] = s^3 \frac{d^3}{ds^3} Q_s(s) + 9s^2 \frac{d^2}{ds^2} Q_s(s) + 18s \frac{d}{ds} Q_s(s) + 6Q_s(s) \tag{14a}$$

$$\frac{d^3}{ds^3}\left[s^2 Q_s(s)\right] = s^2 \frac{d^3}{ds^3} Q_s(s) + 6s \frac{d^2}{ds^2} Q_s(s) + 6 \frac{d}{ds} Q_s(s) \tag{14b}$$

$$\frac{d^3}{ds^3}\left[sQ_{ef}(s)\right] = s \frac{d^3}{ds^3} Q_{ef}(s) + 3 \frac{d^2}{ds^2} Q_{ef}(s) \tag{14c}$$

Replacing the set of equations (13) into equation (12a) yields

$$\begin{aligned} s^3 \frac{d^3}{ds^3} Q_m(s) + 9s^2 \frac{d^2}{ds^2} Q_m(s) + 18s \frac{d}{ds} Q_m(s) + 6Q_m(s) = \\ -a_m \left[s^2 \frac{d^3}{ds^3} Q_m(s) + 6s \frac{d^2}{ds^2} Q_m(s) + 6 \frac{d}{ds} Q_m(s) \right] \\ +b_m \left[s \frac{d^3}{ds^3} U(s) + 3 \frac{d^2}{ds^2} U(s) \right] \\ -g_m \left[s \frac{d^3}{ds^3} Q_{ef}(s) + 3 \frac{d^2}{ds^2} Q_{ef}(s) \right] \end{aligned} \tag{15}$$

and replacing the set of equations (14) into equation (12b) produces

$$\begin{aligned} s^3\frac{d^3}{ds^3}Q_s(s) + 9s^2\frac{d^2}{ds^2}Q_s(s) + 18s\frac{d}{ds}Q_s(s) + 6Q_s(s) = \\ -a_s\left[s^2\frac{d^3}{ds^3}Q_s(s) + 6s\frac{d^2}{ds^2}Q_s(s) + 6\frac{d}{ds}Q_s(s)\right] \\ +g_s\left[s\frac{d^3}{ds^3}Q_{ef}(s) + 3\frac{d^2}{ds^2}Q_{ef}(s)\right] \end{aligned} \tag{16}$$

Multiplying (15) and (16) by s^{-3} and applying the inverse Laplace Transform leads to the next parameterization

$$z_1(t) = a_m\phi_{11}(t) + b_m\phi_{12}(t) + g_m\phi_{13}(t) \tag{17}$$

$$\begin{aligned} z_1(t) &= t^3q_m - 9\int t^2q_m + 18\int^{(2)} tq_m - 6\int^{(3)} q_m \\ \phi_{11}(t) &= -\int t^3q_m + 6\int^{(2)} t^2q_m - 6\int^{(3)} tq_m \\ \phi_{12}(t) &= \int^{(2)} t^3u - 3\int^{(3)} t^2u \\ \phi_{13}(t) &= -\int^{(2)} t^3q_{ef} + 3\int^{(3)} t^2q_{ef} \end{aligned}$$

$$z_2(t) = a_s\phi_{21}(t) + g_s\phi_{22}(t) \tag{18}$$

$$\begin{aligned} z_2(t) &= t^3q_s - 9\int t^2q_s + 18\int^{(2)} tq_s - 6\int^{(3)} q_s \\ \phi_{21}(t) &= -\int t^3q_s + 6\int^{(2)} t^2q_s - 6\int^{(3)} tq_s \\ \phi_{22}(t) &= \int^{(2)} t^3q_{ef} - 3\int^{(3)} t^2q_{ef} \end{aligned}$$

The operator $\int^{(n)}\rho(t)$ represents the iterated integral $\int_0^t\int_0^{\tau_1}\ldots\int_0^{\tau_{n-1}}\rho(\tau_n)d\tau_n\ldots d\tau_2\tau_1$.

APPENDIX D

STABILITY ANALYSIS OF THE PROTOTYPE MODEL (4.8) UNDER STATE FEEDBACK

The model of the whole prototype (4.26) is reproduce here

$$\dot{x}(t) = Ax(t) + bu(t) + s \tag{19}$$

Consider the model (19) without disturbances. Since it has been shown that it is controllable, then there exists a transformation T such that $x(t) = T\bar{x}(t)$. Consequently, this fact allows writing (19) without disturbances as follows

$$\dot{\bar{x}}(t) = \bar{A}x(t) + \bar{b}u(t) \tag{20}$$

where

$$\bar{A} = T^{-1}AT = \begin{bmatrix} 0 & 1 & 0 & 0 \\ 0 & 0 & 1 & 0 \\ 0 & 0 & 0 & 1 \\ -\bar{a}_4 & -\bar{a}_3 & -\bar{a}_2 & -\bar{a}_1 \end{bmatrix}; \qquad \bar{b} = T^{-1}b = \begin{bmatrix} 0 \\ 0 \\ 0 \\ 1 \end{bmatrix}$$

Define the following state feedback

$$\begin{aligned} u &= -\bar{K}^T\bar{x}(t) \\ \bar{K}^T &= \begin{bmatrix} \bar{k}_4 & \bar{k}_3 & \bar{k}_2 & \bar{k}_1 \end{bmatrix} \end{aligned} \tag{21}$$

Substituting (21) into (20) yields

$$\dot{\bar{x}}(t) = \left(\bar{A} - \bar{b}\bar{K}^T\right)\bar{x}(t) \tag{22}$$

Note that

$$-\bar{b}\bar{K}^T = \begin{bmatrix} 0 & 0 & 0 & 0 \\ 0 & 0 & 0 & 0 \\ 0 & 0 & 0 & 0 \\ -\bar{k}_4 & -\bar{k}_3 & -\bar{k}_2 & \bar{k}_1 \end{bmatrix} \tag{23}$$

On the other hand, matrix $\bar{A}$ is decomposed as

$$\bar{A} = \begin{bmatrix} 0 & 1 & 0 & 0 \\ 0 & 0 & 1 & 0 \\ 0 & 0 & 0 & 1 \\ 0 & 0 & 0 & 0 \end{bmatrix} + \begin{bmatrix} 0 & 0 & 0 & 0 \\ 0 & 0 & 0 & 0 \\ 0 & 0 & 0 & 0 \\ -\bar{a}_4 & -\bar{a}_3 & -\bar{a}_2 & -\bar{a}_1 \end{bmatrix} \tag{24}$$

Using (23) and (24) produces the next alternative writing for $\bar{A}_{LC} = \bar{A} - \bar{b}\bar{K}^T$

$$\bar{A}_{LC} = \bar{A}_1 + E \tag{25}$$

with

$$\bar{A}_1 = \begin{bmatrix} 0 & 1 & 0 & 0 \\ 0 & 0 & 1 & 0 \\ 0 & 0 & 0 & 1 \\ -\bar{k}_4 & -\bar{k}_3 & -\bar{k}_2 & -\bar{k}_1 \end{bmatrix}; \qquad E = \begin{bmatrix} 0 & 0 & 0 & 0 \\ 0 & 0 & 0 & 0 \\ 0 & 0 & 0 & 0 \\ -\bar{a}_4 & -\bar{a}_3 & -\bar{a}_2 & -\bar{a}_1 \end{bmatrix} \tag{26}$$

Note that $\bar{A}_1$ is Hurwitz stable if its characteristic polynomial

$$s^4 + k_1 s^3 + k_2 s^2 + k_3 s + k_4 = 0 \tag{27}$$

has roots with negative real part. Moreover, if $\bar{A}_1$ is Hurwitz stable, then it fulfills the Lyapunov equation

$$\bar{A}_1 P_1 + P_1 \bar{A}_1 = -2\mathbb{I} \tag{28}$$

with $P_1 = P_1^T > 0$ and $\mathbb{I} \in \mathbb{R}^{4\times4}$ is the identity matrix. Let $\lambda_i\left(\bar{A}_1\right)$ an eigenvalue of $\bar{A}_1$ and $\mathbb{R}\left(\lambda_i\left(\bar{A}_1\right)\right)$ the real part of $\lambda_i\left(\bar{A}_1\right)$. Then

$$\mu_1 \triangleq \frac{1}{\lambda_{max}(P_1)} = -\delta \tag{29}$$

where $\lambda_{max}(P_1)$ stands for the largest eigenvalue of A_1 and

$$\delta = \max_i \left[\mathbb{R}\left(\lambda_i\left(\bar{A}_1\right)\right)\right] < 0 \tag{30}$$

further details are found in [53]. The Euclidean norm of $\bar{A}_1$ is defined as

$$\left\|\bar{A}_1\right\| = \sqrt{\sum_{i=1}^{4} \bar{k}_i^2 + 3} \tag{31}$$

The magnitude of $\left\|\bar{A}_1\right\|$ grows as the feedback gains increases. Likewise, the Euclidean norm of E is defined as

$$\|E\| = \sqrt{\sum_{i=1}^{4} \bar{a}_i^2} \tag{32}$$

Finally, the Euclidean norm of $\bar{A}_1$ satisfies [54]

$$\left|\mathbb{R}\left(\lambda_i\left(\bar{A}_1\right)\right)\right| \leq \left|\lambda_i\left(\bar{A}_1\right)\right| \leq \left\|\bar{A}_1\right\| \tag{33}$$

which allows writing (30) as

$$\mu_1 \triangleq \frac{1}{\lambda_{max}\left(P_1\right)} = -\delta \leq \left\|\bar{A}_1\right\| = \sqrt{\left\|\bar{k}\right\|^2 + 3} \leq \left\|\bar{k}\right\| + \sqrt{3} \tag{34}$$

The aforementioned results will be used in the next stability analysis. Consider the following Lyapunov Function candidate

$$V(t) = \bar{x}^T(t) P_1 \bar{x}(t) \tag{35}$$

taking the time derivative of (32) and substituting the next representation of (22)

$$\dot{\bar{x}}(t) = \left(\bar{A}_1 + E\right)\bar{x}(t) \tag{36}$$

produces

$$\begin{aligned}\dot{V}(t) &= \dot{\bar{x}}^T(t)P_1\bar{x}(t) + \bar{x}^T(t)P_1\dot{\bar{x}}(t) \\ &= \bar{x}^T(t)\bar{A}_1^T P_1\bar{x}(t) + \bar{x}^T(t)E^T P_1\bar{x}(t) + \bar{x}^T(t)P_1\bar{A}_1\bar{x}(t) + \bar{x}^T(t)P_1E\bar{x}(t) \\ &= \bar{x}^T(t)\left(\bar{A}_1^T P_1 + P_1\bar{A}_1\right)\bar{x}(t) + 2\bar{x}^T(t)P_1E\bar{x}(t)\end{aligned} \tag{37}$$

Substituting (28) yields

$$\dot{V}(t) = -2\bar{x}^T(t)\bar{x}(t) + 2\bar{x}^T(t)P_1E\bar{x}(t) \tag{38}$$

Consider the next inequality

$$2\bar{x}^T(t)P_1E\bar{x}(t) \leq \lambda_{max}(P_1)\,\|E\|\,\|\bar{x}\|^2(t) \tag{39}$$

It allows obtaining an upper bound for (38)

$$\dot{V}(t) \leq -2\|\bar{x}(t)\|^2\left(1 - \lambda_{max}(P_1)\,\|E\|\right) \tag{40}$$

Hence, the system (36) is asymptotically stable provided that

$$1 > \lambda_{max}(P_1)\,\|E\| \tag{41}$$

The above condition is equivalent to

$$\|E\| \leq \frac{1}{\lambda_{max}(P_1)} \leq \left\|\bar{k}\right\| + \sqrt{3} \tag{42}$$

where inequality (34) has been used. Thereby, the closed-loop system (36) is

asymptotically stable provided that

$$\|E\| - \sqrt{3} \leq \left\|\bar{k}\right\| \tag{43}$$

Note that matrix E is unknown, therefore, inequality (43) is fulfilled if the norm $\left\|\bar{k}\right\|$ is high enough.

If matrix E is known beforehand it is not difficult to establish a lower bound for $\left\|\bar{k}\right\|$ fulfilling (43). However, this matrix is poorly or completely unknown in practice, so that the inequality (43) ensures that it is possible in practice to find values of feedback gains high-enough to stabilize the closed-loop system. This argument supports the method used to tune the parallel PD controller (4.32) in Section 4.3. On the other hand, a similar analysis in the perturbed case, i.e. when vector s in (19) is taken into account will show that equilibrium point remains stable.

It is also worth nothing that control law (21) is expressed in the original coordinates as

$$\begin{aligned} u &= -\bar{K}\bar{x}(t) \\ &= -\bar{K}T^{-1}x(t) \\ &= -Kx(t) \end{aligned} \tag{44}$$

APPENDIX E

RAFAEL KELLY AWARD

Figure 3: Rafael Kelly Acknowledgment

REFERENCES

[1] R. Garrido and A. Concha, "An algebraic recursive method for parameter identification of a servo model," *IEEE/ASME Transactions on Mechatronics*, vol. 18, no. 5, pp. 1572–1580, 2013.

[2] R. Garrido and R. Miranda, "Dc servomechanism parameter identification: A closed loop input error approach," *ISA transactions*, vol. 51, no. 1, pp. 42–49, 2012.

[3] R. Garrido and A. Concha, "Inertia and friction estimation of a velocity-controlled servo using position measurements," *IEEE Transactions on industrial electronics*, vol. 61, no. 9, pp. 4759–4770, 2014.

[4] A. Ramírez, R. Garrido, and S. Mondié, "Velocity control of servo systems using an integral retarded algorithm," *ISA transactions*, vol. 58, pp. 357–366, 2015.

[5] C. Aguilar-Ibañez, R. Garrido-Moctezuma, and J. Davila, "Output feedback trajectory stabilization of the uncertainty dc servomechanism system," *ISA transactions*, vol. 51, no. 6, pp. 801–807, 2012.

[6] R. Villafuerte, S. Mondié, and R. Garrido, "Tuning of proportional retarded controllers: Theory and experiments," *IEEE Transactions on Control Systems Technology*, vol. 21, no. 3, pp. 983–990, 2013.

[7] A. Ramírez, S. Mondié, R. Garrido, and R. Sipahi, "Design of proportional-integral-retarded (pir) controllers for second-order lti systems," *IEEE Transactions on Automatic Control*, vol. 61, no. 6, pp. 1688–1693, 2016.

[8] G. Ellis, *Control system design guide: using your computer to understand and diagnose feedback controllers*. Butterworth-Heinemann, 2012.

[9] I. Eker, "Experimental on-line identification of an electromechanical system," *ISA transactions*, vol. 43, no. 1, pp. 13–22, 2004.

[10] S. Villwock and M. Pacas, "Application of the welch-method for the identification of two-and three-mass-systems," *IEEE Transactions on Industrial Electronics*, vol. 55, no. 1, pp. 457–466, 2008.

[11] S. E. Saarakkala, T. Leppinen, M. Hinkkanen, and J. Luomi, "Parameter estimation of two-mass mechanical loads in electric drives," in *Advanced Motion Control (AMC), 2012 12th IEEE International Workshop on*, pp. 1–6, IEEE, 2012.

[12] S. E. Saarakkala and M. Hinkkanen, "Identification of two-mass mechanical systems using torque excitation: Design and experimental evaluation," *IEEE Transactions on industry applications*, vol. 51, no. 5, pp. 4180–4189, 2015.

[13] N. Nevaranta, J. Parkkinen, T. Lindh, M. Niemelä, O. Pyrhönen, and J. Pyrhönen, "Online estimation of linear tooth belt drive system parameters," *IEEE Transactions on Industrial Electronics*, vol. 62, no. 11, pp. 7214–7223, 2015.

[14] A. S. Shafer and M. R. Kermani, "On the feasibility and suitability of mr fluid clutches in human-friendly manipulators," *IEEE/ASME Transactions on Mechatronics*, vol. 16, no. 6, pp. 1073–1082, 2011.

[15] T. Majima, S. Nagai, H. Tomori, and T. Nakamura, "Development of 1-dof manipulator with variable rheological joint for instantaneous force," in *Journal of Physics: Conference Series*, vol. 412, p. 012048, IOP Publishing, 2013.

[16] A. Milecki and D. Sedziak, "The use of magnetorheological fluid dampers to reduce servo drive velocity jumps due to load changes," *Journal of intelligent material systems and structures*, vol. 16, no. 6, pp. 501–510, 2005.

[17] C.-M. Chew, G.-S. Hong, and W. Zhou, "Series damper actuator system based on mr fluid damper," *Robotica*, vol. 24, no. 6, pp. 699–710, 2006.

[18] E. Garcia, J. C. Arévalo, G. Muñoz, and P. Gonzalez-de Santos, "Combining series elastic actuation and magneto-rheological damping for the control of agile locomotion," *Robotics and Autonomous Systems*, vol. 59, no. 10, pp. 827–839, 2011.

[19] Z. Li, Z. Wu, and J. Cui, "Vibration suppression for scara robot with magnetorhelogical damper by using switching control," in *Information and Automation (ICIA), 2014 IEEE International Conference on*, pp. 730–735, IEEE, 2014.

[20] M. Cinq-Mars and H. Gurocak, "Pneumatic cylinder with magnetorheological brake using serpentine and helix flux guide as a linear hybrid actuator for haptics," *Journal of Intelligent Material Systems and Structures*, vol. 28, no. 10, pp. 1303–1321, 2017.

[21] N. Najmaei, M. R. Kermani, and R. V. Patel, "Suitability of small-scale magnetorheological fluid-based clutches in haptic interfaces for improved performance," *IEEE/ASME Transactions on Mechatronics*, vol. 20, no. 4, pp. 1863–1874, 2015.

[22] O. Baser and M. A. Demiray, "Selection and implementation of optimal magnetorheological brake design for a variable impedance exoskeleton robot joint," *Proceedings of the Institution of Mechanical Engineers, Part C: Journal of Mechanical Engineering Science*, vol. 231, no. 5, pp. 941–960, 2017.

[23] L.-H. Zong, X.-L. Gong, S.-H. Xuan, and C.-Y. Guo, "Semi-active h^{∞} control of high-speed railway vehicle suspension with magnetorheological dampers," *Vehicle System Dynamics*, vol. 51, no. 5, pp. 600–626, 2013.

[24] P. Krauze and J. Kasprzyk, "Vibration control in quarter-car model with magnetorheological dampers using fxlms algorithm with preview," in *Control Conference (ECC), 2014 European*, pp. 1005–1010, IEEE, 2014.

[25] S. Dyke, B. Spencer Jr, M. Sain, and J. Carlson, "Modeling and control of magnetorheological dampers for seismic response reduction," *Smart materials and structures*, vol. 5, no. 5, p. 565, 1996.

[26] Q. Fu, D.-H. Wang, L. Xu, and G. Yuan, "A magnetorheological damper-based prosthetic knee (mrpk) and sliding mode tracking control method for an mrpk-based lower limb prosthesis," *Smart Materials and Structures*, vol. 26, no. 4, p. 045030, 2017.

[27] D. Wang and W. H. Liao, "Magnetorheological fluid dampers: a review of parametric modelling," *Smart materials and structures*, vol. 20, no. 2, p. 023001, 2011.

[28] R. Stanway, J. Sproston, and N. Stevens, "Non-linear modelling of an electro-rheological vibration damper," *Journal of Electrostatics*, vol. 20, no. 2, pp. 167–184, 1987.

[29] M. Ismail, F. Ikhouane, and J. Rodellar, "The hysteresis bouc-wen model, a survey," *Archives of Computational Methods in Engineering*, vol. 16, no. 2, pp. 161–188, 2009.

[30] G. Moog Components, "Permanents Magnet DC Motors." `http://www.moog.com/content/dam/moog/literature/MCG/moc23series.pdf`, 2016. [Online; accessed 10-December-2016].

[31] C. Copley Control, "DC Brush Servo Amplifiers." `http://www.copleycontrols.com/Motion/pdf/412.pdf`, 2017. [Online; accessed 24-February-2017].

[32] C. US Digital, "E3 Optical Kit Encoder." `http://cdn.usdigital.com/assets/datasheets/E3_datasheet.pdf?k=636251417279640657`, 2017. [Online; accessed 21-February-2017].

[33] C. Lord, "LORD TFD Steer-by-wire." `http://www.lordmrstore.com/_literature_192930/LORD_SBW_Data_Sheet`, 2017. [Online; accessed 21-February-2017].

[34] C. Lord, "LORD Wonder Box." `http://www.lordmrstore.com/lord-mr-products/wonder-box-device-controller-kit`, 2017. [Online; accessed 21-February-2017].

[35] C. Ogura Industrial, "Electro Magnetic Clutches and Brakes." `http://ogura-clutch.com/downloads/marketbrochures/Industrial_Brochure.pdf`, 2017. [Online; accessed 21-February-2017].

[36] C. ServoTek Products, "SD Tachometer Generatos." http://www.cmggroup.com.au/pdfs/PowerTransmission/CatalogTacho%27s.pdf, 2017. [Online; accessed 21-February-2017].

[37] I. Quanser, "QUARC® Real-Time Control Software." http://www.quanser.com/Products/quarc, 2016. [Online; accessed 10-December-2016].

[38] I. Quanser, "Q8 Data Adquisition Board." http://www.quanser.com/products/q8, 2016. [Online; accessed 10-December-2016].

[39] K. Ogata and G. L. P. Sánchez, *Dinámica de sistemas*. Prentice-Hall Hispanoamericana, 1987.

[40] A. C. Sánchez, *Identificación de Sistemas Mecánicos y Biológicos*. PhD thesis, DCA - CINVESTAV, Av. Instituto Politécnico Nacional 2508, Gustavo A. Madero, San Pedro Zacatenco, 07360 Ciudad de México, CDMX, 8 2013.

[41] L. Ljung, "Consistency of the least-squares identification method," *IEEE Transactions on Automatic Control*, vol. 21, no. 5, pp. 779–781, 1976.

[42] R. Isermann and M. Münchhof, *Identification of Dynamic Systems: An Introduction with Applications*. Springer Publishing Company, Incorporated, 2014.

[43] G. Mamani, J. Becedas, V. Feliu-Batlle, and H. Sira-Ramírez, "Open-and closed-loop algebraic identification method for adaptive control of dc motors," *International journal of adaptive control and signal processing*, vol. 23, no. 12, p. 1097, 2009.

[44] S. J. Miller, "The method of least squares," *Mathematics Department Brown University*, pp. 1–7, 2006.

[45] G. C. Goodwin and K. S. Sin, *Adaptive filtering prediction and control*. Courier Corporation, 2014.

[46] T. Kailath, *Linear systems*, vol. 156. Prentice-Hall Englewood Cliffs, NJ, 1980.

[47] A. Hurwitz, "Ueber die bedingungen, unter welchen eine gleichung nur wurzeln mit negativen reellen theilen besitzt," *Mathematische Annalen*, vol. 46, no. 2, pp. 273–284, 1895.

[48] S. K. Korovin and V. V. Fomichev, *State observers for linear systems with uncertainty*, vol. 51. Walter de Gruyter, 2009.

[49] K. J. Åström and T. Hägglund, *PID controllers: theory, design, and tuning*, vol. 2. Isa Research Triangle Park, NC, 1995.

[50] J. C. Willems and J. W. Polderman, *Introduction to mathematical systems theory: a behavioral approach*, vol. 26. Springer Science & Business Media, 2013.

[51] J. Zabczyk, *Mathematical control theory: an introduction*. Springer Science & Business Media, 2009.

[52] C. L. Phillips and R. D. Habor, *Feedback Control Systems*. Simon & Schuster, 3rd ed., 1995.

[53] R. Patel and M. Toda, "Quantitative measures of robustness for multivariable systems," in *Joint Automatic Control Conference*, no. 17, p. 35, 1980.

[54] P. Lancaster and M. Tismenetsky, *The theory of matrices: with applications*. Elsevier, 1985.